

Supporting Information for

Sequential FRET Processes in Calix[4]arene-Linked Orange-Red-Green Perylene Bisimide Dye Zigzag Arrays

Catharina Hippus[†], Ivo H. M. van Stokkum[¶], Marcel Gsänger[†], Michiel M. Groeneveld[‡], René M. Williams,^{*,‡} and Frank Würthner^{*,†}

Contribution from the [†]Institut für Organische Chemie and Röntgen Research Center for Complex Material Systems, Universität Würzburg, Am Hubland, D-97074 Würzburg, Germany;

[‡]Molecular Photonics Group, van't Hoff Institute for Molecular Sciences (HIMS), Universiteit van Amsterdam, Nieuwe Achtergracht 129, 1018 WV Amsterdam, The Netherlands;

[¶]Department of Physics and Astronomy, Vrije Universiteit, de Boelelaan 1081, 1081 HV Amsterdam, The Netherlands.

E-mail: wuerthner@chemie.uni-wuerzburg.de; williams@science.uva.nl

Materials and Methods:

Perylene bisanhydrides **rPBA**,^{S1} **gPBA**,^{S2} perylene monoimide monoanhydrides **oPMI**,^{S3} **rPMI**,^{S4} **gPMI**,^{S2,S5} as well as precursor compounds **pcA**,^{S6} **pcB**,^{S7} and **pcC**,^{S7} reference compounds **oc**,^{S8} **gc**,^{S7} and arrays **rg**,^{S7} **grorg**^{S7} were synthesized according to literature procedures. Perylene bisanhydride **oPBA** was commercially available. Solvents were purified and dried according to standard procedures. For UV/vis absorption and fluorescence experiments, spectroscopy grade solvents were used. Column chromatography was performed with silica gel 60 (0.035–0.070 mm) and preparative thin layer chromatography (preparative TLC) on 20 x 20 cm plates, height 1 mm, silica gel 60 (0.035–0.070 mm). High performance liquid chromatography (HPLC) was performed on normal phase (NP) SiO₂ columns with p.a. grade solvents as eluants. NMR spectra were recorded on a Bruker 400 MHz spectrometer. Mass spectra were performed on a Finnigan MAT

MS 8200 or on a Bruker microTOF_{LC}. All compounds were characterized by ¹H NMR spectroscopy and high resolution mass spectrometry.

UV/vis absorption spectra were taken on a conventional UV/vis absorption spectrophotometer. **Steady state fluorescence emission** spectra were recorded on a PTI QM4-2003 fluorescence spectrometer and are corrected against photomultiplier and lamp intensity. A long wavelength range emission corrected photomultiplier R928 was used. Fluorescence quantum yields were determined in CH₂Cl₂ vs. *N,N'*-bis(2,6-diisopropylphenyl)-1,6,7,12-tetraphenoxyperylene-3,4:9,10-tetracarboxylic acid bisimide ($\Phi_{fl} = 0.96$ in CHCl₃) or Fluorescein ($\Phi_{fl} = 0.92$ in 0.1N NaOH) or Nile blue perchlorate ($\Phi_{fl} = 0.27$ in ethanol) as reference.^{S9} The given quantum yields are averaged from values measured at three different excitation wavelengths with OD 0.02–0.05 in the absorption maximum (standard deviation $\sigma = 1$ –3%).

Femtosecond transient absorption experiments were performed with a Spectra-Physics Hurricane Titanium: Sapphire regenerative amplifier system.^{S10} The full spectrum setup was based on an optical parametric amplifier (Spectra-Physics OPA 800) as the pump. The residual fundamental light from the pump OPA was used for white light generation, which was detected with a CCD spectrograph (Ocean Optics). The polarization of the pump light was controlled by a Berek Polarization Compensator (New Focus). The Berek-Polarizer was always included in the setup to provide the magic-angle conditions. The probe light was passed over a delay line (Physik Instrumente, M-531DD) that provides an experimental time window of 1.0 ns with a maximal resolution of 0.6 fs/step. The OPA was used to generate excitation pulses at 530 nm. The laser output was typically 5 mJ pulse⁻¹ (130 fs FWHM) with a repetition rate of 1 kHz. The samples were placed into cells of 2 mm path length (Hellma) and were stirred with a stir bar. Samples were prepared to have an optical density of *ca.* 0.3–0.6 at the excitation wavelength and were degassed for 15 minutes with argon gas prior to the measurements. The UV/vis absorption spectra of the samples were measured before and after the laser experiments and were virtually identical, thus possible degradation or chemical change of the samples could be ruled out. All photophysical data reported here have a 5 to 10% error limit, unless indicated otherwise. The experiments were performed at room temperature. The power dependence was determined and it was found that the spectral and kinetic behavior was independent of the laser power used. Four different laser powers were applied by modulating the maximum laser power of the pump beam with a neutral density filter wheel.

For the **global and target analysis**, all time-gated spectra were collated in a matrix, which was globally fitted using a sequential kinetic scheme with increasing lifetimes. From this the lifetimes and the evolution-associated difference spectra (EADS) were estimated. The instrument response function (IRF) is described by a Gaussian shape, and the white light dispersion over the spectral range is modeled by a third order polynomial. With increasing lifetimes, and thus decreasing rates, the first EADS decays with the first lifetime and corresponds to the difference spectrum at time zero with an ideal infinitely small IRF. The second EADS is formed with the first lifetime and decays with the second lifetime, etc. The final EADS represents the difference spectrum of the longest living species. The error in the lifetimes obtained from the fitting procedure does not exceed 10%. EADS may not represent pure species, except for the final EADS, and they are interpreted as a weighted sum (with only positive contributions) of species-associated difference spectra (SADS). The quality of the fit was judged by inspection of the singular vectors of the matrix of residuals, which had to be structure-less. Next, in target analysis a kinetic scheme was used in combination with spectral assumptions to estimate microscopic rate constants and SADS. A full description of the method has been given elsewhere.^{S11}

Synthesis and Chemical characterization.

Compound **pcD**:

A solution of 110 mg (1.52×10^{-2} mmol, 1 equiv.) of calix[4]arene compound **pcA**, 190 mg (1.83×10^{-2} mmol, 1.2 equiv.) of **rPMI** were heated under an argon atmosphere to 110 °C for 23 h together with 5 drops of triethylamine in toluene (1.5 mL). The solvent was evaporated, the remaining crude product purified by column chromatography with CH₂Cl₂/hexane 70:30 and precipitated from CH₂Cl₂/methanol. Compound **pcD** was obtained as a red powder (101 mg, 5.79×10^{-3} mmol, yield 38%). C₁₁₃H₁₂₁N₃O₁₄ (1745.18). Mp = 295 – 296 °C. TLC: CH₂Cl₂/hexane 80:20; R_f = 0.54. **¹H NMR** (400 MHz, CDCl₃, TMS, 25 °C): δ (ppm) = 8.27 and 8.24 (bs and s, 4H; Per-*H*); 7.25 – 7.20 (m, 8H; Phen-*H*); 7.06 (s, 2H; Ar-*H*); 6.95 (s, 2H; Ar-*H*); 6.87 – 6.82 (m, 8H; Phen-*H*); 6.42 (bs, 1H; Boc-N-*H*); 6.26 (t, 2H, ³J = 7.5 Hz; Ar-*H*); 6.19 – 6.15 (m, 4H; Ar-*H*); 4.44 and 3.10 (AX, 4H, ²J = 13.5 Hz; Ar-CH₂-Ar); 4.39 and 3.09 (AX, 4H, ²J = 13.6 Hz; Ar-CH₂-Ar); 4.12 (t, 2H, ³J = 7.2 Hz; N-CH₂); 4.05 – 4.01 and 3.95 – 3.91 (each m, 4H; O-CH₂); 3.66 – 3.62 (m, 4H; O-CH₂); 1.79 (m, 8H; Propyl-*H*); 1.70 – 1.62 (m, 2H, Butyl-*H*); 1.51 (s, 9H; Boc-*tert*-Butyl-*H*); 1.44 – 1.35 (m, 2H, Butyl-*H*); 1.29 and 1.27 (each s, 36H, *tert*-Butyl-Phen-*H*); 1.06 (t, 6H, ³J = 7.4 Hz; Propyl-*H*); 0.94 (t, 3H, ³J = 7.3 Hz; Butyl-*H*); 0.86 and 0.85 (each t, 6H, each ³J = 7.5 Hz; Propyl-*H*). **¹³C NMR** (100 MHz, CDCl₃, TMS, 25 °C): δ (ppm) = 163.6 (C=O), 156.2, 156.1 (br), 155.4, 153.1 (br), 147.5, 137.7, 137.4, 133.2, 133.1, 133.0, 132.1, 128.5, 128.4, 127.7, 127.6, 126.8, 122.7, 122.6, 120.7, 120.1, 119.9, 119.6, 119.5, 77.4 (Boc-*tert*-Butyl-*C*), 76.9, 76.7, 76.6 (O-CH₂ and N-CH₂), 34.5 (Phen-*tert*-Butyl-*C*), 31.6 (CH₃-*tert*-Butyl), 31.2, 30.3 (Ar-CH₂-Aryl); 23.6, 23.0, 20.5, 13.9, 10.9, 10.0, 9.9. **HR-MS** (ESI in THF/CHCl₃): calcd for C₁₁₃H₁₂₅N₄O₁₄ [M+NH₄]⁺ (m/z) 1761.9192; found 1761.9187. **UV/vis** (CH₂Cl₂): λ (nm) [ε (M⁻¹cm⁻¹)] = 579 [45600]. **Fluorescence** (CH₂Cl₂): λ_{max} (nm) = 610; Φ_{Fl} = 0.73.

Array *or*:

A portion of 36 mg (2.05×10^{-2} mmol, 1 equiv.) of compound **pcD** was dissolved in 2 mL dry CH₂Cl₂ and 3 mL of CF₃COOH were added under an argon atmosphere. The mixture was stirred for 1 hour at room temperature, poured into ice water and adjusted to pH > 9 with NH₃ solution (25%). CH₂Cl₂ (50 mL) was added to the reaction mixture, the two phases were separated, and the organic phase was washed with water and brine and dried over Na₂SO₄. The solvent was removed under vacuum and the resulting crude product (32 mg; 1.95×10^{-2} mmol) dried and used without further purification.

Under an argon atmosphere 32 mg (1.95×10^{-2} mmol, 1 equiv.) of the obtained crude product, 21 mg (3.89×10^{-2} mmol, 2 equiv.) of compound **oPMI** and 7 mg (3.89×10^{-2} mmol, 2 equiv.) of $\text{Zn}(\text{OAc})_2$ (H_2O -free) were heated in quinoline (0.60 mL) at 170 °C for 12.5 h. The cooled reaction mixture was poured into 30 mL of 2N HCl and stirred for 30 minutes at 50 °C. The resulting precipitate was filtered and dissolved in CH_2Cl_2 . The solution was washed with water and brine and dried over MgSO_4 . The crude product was purified first by column chromatography with CH_2Cl_2 and successively by HPLC with CH_2Cl_2 (SiO_2 , normal phase) and precipitation from CH_2Cl_2 /methanol. Compound **or** was obtained as a red powder (10 mg, 4.60×10^{-3} mmol, yield 23% over two steps). $\text{C}_{143}\text{H}_{142}\text{N}_4\text{O}_{16}$ (2172.67). Mp = 370 – 372 °C. TLC: CH_2Cl_2 ; $R_f = 0.10$. $^1\text{H NMR}$ (400 MHz, CDCl_3 , 25 °C): δ (ppm) = 8.78 and 8.69 – 8.52 (d and m, 8H, $^3\text{J} = 7.8$ Hz; Per-*H*); 8.29 and 8.23 (bs and s, 4H; Per-*H*); 7.25 – 7.22 (m, 8H; Phen-*H*); 7.10 (s, 2H; Ar-*H*); 7.02 (s, 2H; Ar-*H*); 6.88 – 6.84 (m, 8H; Phen-*H*); 6.35 (t, 2H, $^3\text{J} = 7.5$ Hz; Ar-*H*); 6.20 and 6.15 (each d, 4H, $^3\text{J} = 7.7$ Hz and 7.5 Hz; Ar-*H*); 5.23 – 5.16 (m, 1H, N-*CH*); 4.51 and 3.19 (each AX, 4H, $^2\text{J} = 14.0$ Hz and 12.8 Hz; Ar- CH_2 -Ar); 4.47 and 3.16 (each AX, 4H, $^2\text{J} = 14.3$ Hz and 13.0 Hz; Ar- CH_2 -Ar); 4.14 – 4.06 (m, 6H; O- CH_2 and N- CH_2); 3.64 (t, 4H, $^3\text{J} = 6.6$ Hz; O- CH_2); 2.30 – 2.21 (m, 2H; Alkyl-*H*); 2.04 – 1.82 (m, 10H; Alkyl-*H*); 1.67 – 1.62 (m, 2H, Alkyl-*H*); 1.42 – 1.36 (m, 2H, Alkyl-*H*); 1.31 – 1.29 (m and two s, 48H, *tert*-Butyl-Phen-*H* and Alkyl-*H*); 1.09 (t, 6H, $^3\text{J} = 7.4$ Hz; Alkyl-*H*); 0.96 – 0.82 (m, 15H; Alkyl-*H*). **HR-MS** (ESI in acetonitrile/ CHCl_3): calcd for $\text{C}_{143}\text{H}_{142}\text{N}_4\text{NaO}_{16} [\text{M}+\text{Na}]^+$ (m/z) 2194.0319; found 2194.0313. **UV/vis** (CH_2Cl_2): λ (nm) [ϵ ($\text{M}^{-1}\text{cm}^{-1}$)] = 579 [46200], 526 [107900], 489 [62000], 457 [34900]. **Fluorescence** (CH_2Cl_2): λ_{max} (nm) = 608 with $\lambda_{\text{ex}} = 490$ nm; $\Phi_{\text{Fl}} = 0.72$.

Compound pcE:

A solution of 100 mg (1.38×10^{-2} mmol, 1 equiv.) of calix[4]arene-compound **pcA**, 169 mg (2.76×10^{-2} mmol, 2 equiv.) of **gPMI** and 51 mg (2.76×10^{-2} mmol, 2 equiv.) of $\text{Zn}(\text{OAc})_2$ (H_2O -free) was heated in quinoline (1.5 mL) at 130 °C for 20 h. The cooled reaction mixture was poured into 40 mL of 1N HCl and stirred for 40 minutes at 50 °C. The resulting precipitate was filtered and dissolved in CH_2Cl_2 . The solution was washed with water and brine and dried over MgSO_4 . The crude product was purified by column chromatography with CH_2Cl_2 and subsequent precipitation from CH_2Cl_2 /methanol. Compound **pcE** was obtained as a dark-green powder (24 mg, 1.97×10^{-3} mmol, yield 14%). It is to note, that these reaction conditions lead to the NH_2 -functionalized Calix[4]arene–PBI array **pcE**, and not the expected Boc-functionalized compound, as the Boc-

group is cleaved under the applied reaction conditions. $C_{78}H_{81}N_5O_8$ (1216.51). Mp = 356 °C (dec.). TLC: CH_2Cl_2 /ethyl acetate 95:5; R_f = 0.20. 1H NMR (400 MHz, $CDCl_3$, TMS, 25 °C): δ (ppm) = 8.55 (bs, 1H; Per-*H*); 8.47 and 8.45 (d and s, 2H, 3J = 8.1 Hz; Per-*H*); 8.40 (d, 1H, 3J = 8.1 Hz; Per-*H*); 7.74 and 7.71 (each d, 2H, 3J = 8.2 and 8.1 Hz; Per-*H*); 7.02 (s, 2H; Ar-*H*); 6.43 – 6.30 (m, 8H; Ar-*H*); 5.11 – 5.04 (m, 1H; N-*CH*); 4.51 and 3.18 (AX, 4H, 2J = 13.4 Hz; Ar- CH_2 -Ar); 4.40 and 3.03 (AX, 4H, 2J = 13.4 Hz; Ar- CH_2 -Ar); 4.07 (t, 2H, 3J = 8.1 Hz; O- CH_2); 3.90, 3.75, and 3.70 (t, bs, and t, respectively, 10H, 3J = 8.0 Hz and 6.7 Hz; Pyrr-*H* und O- CH_2); 2.85 (bs, 4H; Pyrr-*H*); 2.65 – 2.57 (m, 2H; Cy-*H*); 2.06 – 1.73 (m, 23H; Pyrr-*H*, Propyl-*H*, Cy-*H*, NH_2); 1.53 – 1.30 (m, 3H; Cy-*H*); 1.08 (t, 6H, 3J = 7.5 Hz; Propyl-*H*); 0.93 and 0.91 (each t, 6H, 3J = 7.6 Hz; Propyl-*H*). MS (FAB in NPOE): calcd for $C_{78}H_{81}N_5O_8$ $[M]^+$ (m/z) 1215.6; found 1215.6. HR-MS (ESI in acetonitrile/ $CHCl_3$): calcd for $C_{78}H_{82}N_5O_8$ $[M+H]^+$ (m/z) 1216.6162; found 1216.6158. UV/vis (CH_2Cl_2): λ (nm) $[\epsilon$ ($M^{-1}cm^{-1}$)] = 706 [42700]. Fluorescence (CH_2Cl_2): λ_{max} (nm) = 744; Φ_{Fl} = 0.04.

Array og:

A solution of 21 mg (1.72×10^{-2} mmol, 1 equiv.) of **pcE**, 19 mg (3.45×10^{-2} mmol, 2 equiv.) of **oPMI** and 7 mg (3.45×10^{-2} mmol, 2 equiv.) of $Zn(OAc)_2$ (H_2O -free) was heated in quinoline (0.3 mL) at 155 °C for 15 h. The cooled reaction mixture was poured into 50 mL of 2N HCl and stirred for 30 minutes at 40 °C. CH_2Cl_2 (50 mL) was added to the reaction mixture, the resulting two phases were separated, and the organic phase was washed with water and brine and dried over Na_2SO_4 . The crude product was purified first by column chromatography with CH_2Cl_2 /ethyl acetate 97:3 and successively by HPLC with CH_2Cl_2 (SiO_2 , normal phase) and precipitation from CH_2Cl_2 /methanol. Compound **og** was obtained as a light-green powder (7 mg, 4.01×10^{-3} mmol, yield 23%). $C_{113}H_{110}N_6O_{12}$ (1744.12). Mp > 400 °C. TLC: CH_2Cl_2 ; R_f = 0.07. 1H NMR (400 MHz, $CDCl_3$, 25 °C) δ (ppm) = 8.79 (bd, 2H, 3J = 7.9 Hz; Per-*H*); 8.68 – 8.64 (m and s, 7H; Per-*H*); 8.53 – 8.50 (s and bd, 2H, 3J = 7.8 Hz; Per-*H*); 8.42 (d, 1H, 3J = 8.0 Hz; Per-*H*); 7.79 and 7.78 (each d, 2H, each 3J = 8.0 Hz; Per-*H*); 7.14 and 7.13 (each s, 4H; Ar-*H*); 6.44 (t, 2H, 3J = 7.5 Hz; Ar-*H*); 6.30 and 6.28 (each bd, 4H, 3J = 8.0 Hz and 7.8 Hz; Ar-*H*); 5.23 – 5.16 and 5.11 – 5.04 (each m, 2H; N-*CH* and Cy-*H*); 4.55 and 3.21 (AX, 4H, 2J = 13.6 and 13.8 Hz; Ar- CH_2 -Ar); 4.54 und 3.21 (AX, 4H, 2J = 13.5 und 13.8 Hz; Ar- CH_2 -Ar); 4.17 – 4.12 (m, 4H; O- CH_2); 3.78 and 3.68 (bs and t, 8H, 3J = 6.5 Hz; Pyrr-*H* and O- CH_2); 2.88 and 2.63 – 2.59 (bs and m, 6H; Pyrr-*H*, Cy-*H*); 2.29 – 2.22 (m, 2H; Alkyl-*H*); 2.13 – 1.83 (m, 20H; Pyrr-*H*, Cy-*H*, Alkyl-*H*); 1.79 – 1.73 (m, 3H; Cy-*H*); 1.50 – 1.28 (m, 15H; Cy-*H*, Alkyl-*H*); 1.12 (t, 6H, 3J = 7.5 Hz; Alkyl-*H*); 0.94 und 0.93 (each t, 6H,

each $^3J = 7.5$ Hz Alkyl-*H*); 0.84 (t, 6H, $^3J = 7.0$ Hz; Alkyl-*H*). **HR-MS** (ESI in acetonitrile/ CHCl_3): calcd for $\text{C}_{113}\text{H}_{110}\text{N}_6\text{O}_{12}$ $[\text{M}]^+$ (m/z) 1742.8182; found 1742.8176. **UV/vis** (CH_2Cl_2): λ (nm) [ϵ ($\text{M}^{-1}\text{cm}^{-1}$)] = 700 [45200], 525 [89600], 489 [56400]. **Fluorescence** (CH_2Cl_2): λ_{max} (nm) = 741 with λ_{ex} = 490 nm; $\Phi_{\text{fl}} = 0.12$.

Array oro:

To a solution of 115 mg (4.79×10^{-2} mmol) of compound **pcB** in 2 mL dry CH_2Cl_2 were added 3 mL of CF_3COOH under an argon atmosphere. The mixture was stirred for 1 h at room temperature, poured into ice water and adjusted to pH > 9 with NH_3 solution (25%). CH_2Cl_2 (50 mL) was added to the mixture, and the resulting organic phase washed with water and brine, and dried over Na_2SO_4 . The solvent was evaporated and the resulting crude product (102 mg; 4.65×10^{-2} mmol) dried and used without further purification.

Under an argon atmosphere 102 mg (4.65×10^{-2} mmol, 1 equiv.) of the obtained crude product, 101 mg (1.86×10^{-2} mmol, 4 equiv.) of **oPMI** and 34 mg ($1.86 \cdot 10^{-5}$ mol, 4 equiv.) of $\text{Zn}(\text{OAc})_2$ (H_2O -free) were heated in quinoline (1.0 mL) at 175 °C for 12.5 h. The cooled reaction mixture was poured into 40 mL of 2N HCl and stirred for 40 minutes at 50 °C. CH_2Cl_2 (50 mL) was added to the reaction mixture, the resulting two phases were separated, and the organic phase was washed with water and brine and dried over MgSO_4 . The crude product was purified first by column chromatography with CH_2Cl_2 and successively by HPLC with CH_2Cl_2 (SiO_2 , normal phase) and finally by precipitation from CH_2Cl_2 /methanol. Compound **oro** was obtained as a red powder (59 mg, 1.81×10^{-2} mmol, yield 38% over two steps). $\text{C}_{214}\text{H}_{210}\text{N}_6\text{O}_{24}$ (3249.98). Mp > 400 °C. TLC: CH_2Cl_2 ; $R_f = 0.67$. **^1H NMR** (400 MHz, CDCl_3 , 25 °C) δ (ppm) = 8.75 and 8.71 – 8.65 (bd and m, 16H; Per-*H*); 8.33 (bs, 4H; Per-*H*); 7.26 (bd, 8H; Phen-*H*, $^3J = 8.7$ Hz); 7.14 (s, 4H; Ar-*H*); 7.05 (s, 4H; Ar-*H*); 6.89 (bd, 8H; Phen-*H*, $^3J = 8.3$ Hz); 6.37 (t, 4H, $^3J = 7.6$ Hz; Ar-*H*); 6.24 and 6.18 (each d, 8H, each $^3J = 7.2$ Hz; Ar-*H*); 5.22 – 5.18 (m, 2H, N-*CH*); 4.52 and 3.19 (each AX, each 4H, $^2J = 13.6$ Hz and 14.3 Hz; Ar- CH_2 -Ar); 4.49 and 3.16 (each AX, each 4H, $^2J = 13.4$ Hz and 14.9 Hz; Ar- CH_2 -Ar); 4.14 – 4.07 (m, 8H; O- CH_2); 3.66 (t, 8H, $^3J = 6.2$ Hz; O- CH_2); 2.29 – 2.25 (m, 4H; Alkyl-*H*); 2.04 – 1.81 (m, 20H; Alkyl-*H*); 1.36 – 1.24 (m, 60H, Alkyl-*H* und *tert*-Butyl-Phen-*H*); 1.10 (t, 12H, $^3J = 7.4$ Hz; Alkyl-*H*); 0.96 – 0.82 (m, 24H; Alkyl-*H*). **HR-MS** (ESI in acetonitrile): calcd for $\text{C}_{214}\text{H}_{210}\text{N}_6\text{Na}_2\text{O}_{24}$ $[\text{M}+2\text{Na}]^{2+}$ (m/z) 1646.7596; found 1646.7591. **Analysis:** calcd (%) for $\text{C}_{214}\text{H}_{210}\text{N}_6\text{O}_{24} \times \text{CH}_3\text{OH}$ (3282.03): C 78.68; H 6.57; N 2.56; found: C 78.98; H 6.94; N 2.51.

UV/vis (CH₂Cl₂): λ (nm) [ϵ (M⁻¹cm⁻¹)] = 580 [50300], 526 [194900], 489 [117500] 458 [57100].

Fluorescence (CH₂Cl₂): λ_{\max} (nm) = 611 with λ_{ex} = 490 nm; Φ_{fl} = 0.72.

Array *ror*:

A portion of 73 mg (4.22×10^{-2} mmol, 1 equiv.) of compound **pcD** was dissolved in 2 mL dry CH₂Cl₂ and 3 mL of CF₃COOH were added under an argon atmosphere. The mixture was stirred for 1 hour at room temperature, poured into ice water and adjusted to pH > 9 with NH₃ solution (25%). CH₂Cl₂ (50 mL) was added to the reaction mixture, the two phases were separated, and the organic phase was washed with water and brine and dried over Na₂SO₄. The solvent was removed and the resulting crude product (68 mg; 4.13×10^{-2} mmol) dried and used without further purification.

A solution of 68 mg (4.13×10^{-2} mmol, 2 equiv.) of the obtained crude product, 8 mg (2.07×10^{-2} mmol, 1 equiv.) of **oPBA** and 15 mg (8.27×10^{-2} mmol, 4 equiv.) of Zn(OAc)₂ (H₂O-free) were heated under an argon atmosphere in quinoline (4.0 mL) at 160 °C for 15.5 h. The cooled reaction mixture was poured into 50 mL of 2N HCl and stirred for 30 minutes at 40 °C. CH₂Cl₂ (50 mL) was added to the reaction mixture, the resulting two phases were separated, and the organic phase was washed with water and brine and dried over MgSO₄. The crude product was purified first by column chromatography with CH₂Cl₂/ethyl acetate 99:1 and successively by HPLC with CH₂Cl₂ (SiO₂, normal phase) and precipitation from CH₂Cl₂/methanol. Compound **ror** was obtained as a red powder (27 mg, 7.41×10^{-3} mmol, yield 35% over two steps). C₂₄₀H₂₃₀N₆O₂₈ (3646.42). Mp > 400 °C. TLC: CH₂Cl₂/ethyl acetate 99:1; R_f = 0.20. **¹H NMR** (400 MHz, CDCl₃, TMS, 25 °C): δ (ppm) = 8.80 and 8.73 (each d, 8H, ³J = 7.8 and 8.2 Hz; Per-*H*); 8.29 and 8.24 (bs and s, 8H; Per-*H*); 7.24 – 7.22 (m, 16H; Phen-*H*); 7.11 (s, 4H; Ar-*H*); 7.02 (s, 4H; Ar-*H*); 6.87 – 6.84 (m, 16H; Phen-*H*); 6.36 (t, 4H, ³J = 7.3 Hz; Ar-*H*); 6.23 and 6.17 (each d, 8H, ³J = 7.5 and 7.2 Hz; Ar-*H*); 4.51 and 3.18 (each AX, each 4H, ²J = 13.4 Hz and 14.3 Hz; Ar-CH₂-Ar); 4.47 and 3.14 (each AB, each 4H, ²J = 13.6 Hz and 14.3 Hz; Ar-CH₂-Ar); 4.14 – 4.06 (m, 12H; O-CH₂ and N-CH₂); 3.65 (t, 8H, ³J = 6.4 Hz; O-CH₂); 2.03 – 1.80 (m, 16H; Propyl-*H*); 1.70 – 1.63 (m, 4H; Butyl-*H*); 1.45 – 1.37 (m, 4H; Butyl-*H*); 1.30 and 1.29 (each s, 72H, *tert*-Butyl-Phen-*H*); 1.09 (t, 12H, ³J = 7.4 Hz; Propyl-*H*); 0.94, 0.91, and 0.87 (each t, 18H, ³J = 7.3 Hz, 7.5 Hz, and 7.5 Hz, respectively; Propyl-*H* und Alkyl-*H*). **HR-MS** (ESI in CHCl₃/acetonitrile): calcd for C₂₄₀H₂₃₈N₈O₂₈ [M+2NH₄]²⁺ (m/z) 1839.8722; found 1839.8717. **Analysis**: calcd (%) for C₂₄₀H₂₃₀N₆O₂₈ x H₂O (3664.43): C 78.66; H 6.38; N 2.29; found: C 78.49; H 6.69; N 2.32. **UV/vis** (CH₂Cl₂): λ (nm) [ϵ (M⁻¹cm⁻¹)] = 578

[91600]; 527 [135000]; 491 [77000], 457 [51600]. **Fluorescence** (CH₂Cl₂): λ_{max} (nm) = 608 with λ_{ex} = 490 nm; Φ_{fl} = 0.71.

Array rgr:

A portion of 73 mg (4.22×10^{-2} mmol, 1 equiv.) of compound **pcD** was dissolved in 2 mL dry CH₂Cl₂ and 3 mL of CF₃COOH were added under an argon atmosphere. The mixture was stirred for 1 hour at room temperature, poured into ice water and adjusted to pH > 9 with NH₃ solution (25%). CH₂Cl₂ (50 mL) was added to the reaction mixture, the two phases were separated, and the organic phase was washed with water and brine and dried over Na₂SO₄. The solvent was removed and the resulting crude product (68 mg; 4.13×10^{-2} mmol) dried and used without further purification.

Under an argon atmosphere 68 mg (4.13×10^{-2} mmol, 2 equiv.) of the obtained crude product, 11 mg (2.07×10^{-2} mmol, 1 equiv.) of **gPBA** and 15 mg (8.27×10^{-2} mmol, 4 equiv.) of Zn(OAc)₂ (H₂O-free) were heated in distilled quinoline (4.0 mL) at 160 °C for 15.5 h. The cooled reaction mixture was poured into 50 mL of 2N HCl and stirred for 30 minutes at 40 °C. CH₂Cl₂ (50 mL) was added to the reaction mixture, the resulting two phases were separated, and the organic phase was washed with water and brine and dried over MgSO₄. The crude product was purified first by column chromatography with CH₂Cl₂/ethyl acetate 99:1 and successively by HPLC with CH₂Cl₂ (SiO₂, normal phase) and finally by precipitation from CH₂Cl₂/methanol. Array **ror** was obtained as a dark-violet powder (24 mg, 6.34×10^{-3} mmol, yield 30% over two steps). C₂₄₈H₂₄₄N₈O₂₈ (3784.63). Mp > 400 °C. TLC: CH₂Cl₂/ethyl acetate 99:1; R_f = 0.44. **¹H NMR** (400 MHz, CDCl₃, TMS, 25 °C): δ (ppm) = 8.62 (bs, 2H; Per-*H*); 8.55 (bd, 2H, ³J = 6.6 Hz; Per-*H*); 8.31 and 8.26 (bs and s, 8H; Per-*H*); 7.85 (bd, 2H, ³J = 7.5 Hz; Per-*H*); 7.26 – 7.22 (m, 16H; Phen-*H*); 7.11 and 7.03 (each s, 8H; Ar-*H*); 6.88 – 6.84 (m, 16H; Phen-*H*); 6.35 (t, 4H, ³J = 7.5 Hz; Ar-*H*); 6.24 (d, 4H, ³J = 7.1 Hz; Ar-*H*); 6.15 (d, 4H, ³J = 6.5 Hz; Ar-*H*); 4.51 and 3.18 (each AX, each 4H, ²J = 13.1 Hz and 14.7 Hz; Ar-CH₂-Ar); 4.48 and 3.14 (each AX, each 4H, ²J = 13.5 Hz and 14.0 Hz; Ar-CH₂-Ar); 4.14 – 4.07 (m, 12H; O-CH₂ and N-CH₂); 3.82 and 3.64 (bs and t, 12H, ³J = 6.6 Hz; Pyrr-*H*, O-CH₂); 2.91 (bs, 4H; Pyrr-*H*); 2.10 – 1.80 (m, 24H; Pyrr-*H*, Propyl-*H*); 1.70 – 1.62 (m, 4H; Alkyl-*H*); 1.45 – 1.36 (m, 4H; Alkyl-*H*); 1.30 and 1.29 (each s, 72H; *tert*-Butyl-Phen-*H*); 1.10 (t, 12H, ³J = 7.4 Hz; Propyl-*H*); 0.96 – 0.86 (m, 18H; Propyl-*H* and Alkyl-*H*). **HR-MS** (ESI in CHCl₃/acetonitrile): calcd for C₂₄₈H₂₅₂N₁₀O₂₈ [M+2NH₄]²⁺ (m/z) 1908.9301; found 1908.9296.

UV/vis (CH₂Cl₂): λ (nm) [ϵ (M⁻¹cm⁻¹)] = 703 [43700], 579 [93700], 436 [45300]. **Fluorescence** (CH₂Cl₂): λ_{max} (nm) = 739 with λ_{ex} = 560 nm; Φ_{fl} = 0.19.

Array grg:

To a solution of 75 mg (3.15×10^{-2} mmol) of compound **pcB** in 1.5 mL dry CH₂Cl₂ were added 3 mL of CF₃COOH under an argon atmosphere. The mixture was stirred for 1 h at room temperature, poured into ice water and adjusted to pH > 9 with NH₃ solution (25%). CH₂Cl₂ (50 mL) was added to the mixture, and the resulting organic phase washed with water and brine and dried over Na₂SO₄. The solvent was evaporated and the resulting crude product (65 mg; 2.96×10^{-2} mmol) dried and used without further purification.

A solution of 62 mg (2.82×10^{-2} mmol, 1 equiv.) of the obtained crude product, 26 mg (4.24×10^{-2} mmol, 1.5 equiv.) of **gPMI** and 10 mg (5.65×10^{-5} mmol, 2 equiv.) of Zn(OAc)₂ (H₂O-free) in distilled quinoline (2.5 mL) was heated under an argon atmosphere at 140 °C for 15 h. The cooled reaction mixture was poured into 20 mL of 1N HCl and stirred for 30 min at 50 °C. CH₂Cl₂ (20 mL) was added to the reaction mixture, the resulting two phases were separated, and the organic phase was washed with water and brine and dried over MgSO₄. The crude product was purified first by column chromatography with CH₂Cl₂/ethyl acetate 99:1 and successively by preparative TLC with CH₂Cl₂/ethyl acetate 99:1 and by HPLC with CH₂Cl₂ (SiO₂, normal phase), and finally by precipitation from CH₂Cl₂/methanol. Array **grg** was obtained as a dark-blue powder (20 mg, 5.91×10^{-3} mmol, yield 18% over two steps). C₂₂₀H₂₁₄N₁₀O₂₄ (3382.11). Mp > 500 °C. TLC: CH₂Cl₂/ethyl acetate 98:2; R_f = 0.96. ¹H NMR (400 MHz, CDCl₃, TMS, 25 °C): δ (ppm) = 8.59 (bs, 2H; Per-*H*); 8.51 – 8.49 (m, 4H, Per-*H*); 8.42 and 8.33 (d and bs, 6H, ³J = 8.1 Hz; Per-*H*); 7.78 – 7.76 (m, 4H; Per-*H*); 7.26 – 7.24 (m, 8H; Phen-*H*); 7.11 and 7.05 (each s, each 4H; Ar-*H*); 6.90 – 6.89 (m, 8H; Phen-*H*); 6.36 (t, 4H, ³J = 7.5 Hz; Ar-*H*); 6.24 (d, 4H, ³J = 7.1 Hz; Ar-*H*); 6.17 (d, 4H, ³J = 7.3 Hz; Ar-*H*); 5.11 – 5.05 (m, 2H; Cy-*H*); 4.51 and 3.18 (each AX, each 4H, ²J = 13.1 Hz; Ar-CH₂-Ar); 4.48 and 3.15 (each AX, each 4H, ²J = 12.6 Hz; Ar-CH₂-Ar); 4.14 – 4.07 (m, 8H; O-CH₂); 3.78 and 3.65 (bs and t, 16H, ³J = 6.3 Hz; Pyrr-*H*, O-CH₂); 2.87 (bs, 8H; Pyrr-*H*); 2.65 – 2.57 (m, 4H; Cy-*H*); 2.08 – 1.76 (m, 42H; Pyrr-*H*, Propyl-*H*, Cy-*H*); 1.50 – 1.37 (m, 6H; Cy-*H*); 1.30 (s, 36H; *tert*-Butyl-Phen-*H*); 1.01 (t, 12H, ³J = 7.4 Hz; Propyl-*H*); 0.91 and 0.87 (each t, 12H, each ³J = 7.4 Hz; Propyl-*H*). **MS** (MALDI in dithranol): calcd for C₂₂₀H₂₁₅N₁₀O₂₄ (m/z) 3380.6 [M+H]⁺ and for C₂₂₀H₂₁₄N₁₀O₂₄K (m/z) 3418.5 [M+K]⁺; found 3380 and 3419. **HR-MS** (ESI in CHCl₃/acetonitrile): calcd for C₂₂₀H₂₁₄N₁₀O₂₄ (m/z) 1689.7916 [M]²⁺; found 1689.7911. **UV/vis** (CH₂Cl₂): λ (nm)

$[\epsilon \text{ (M}^{-1}\text{cm}^{-1})] = 701 [84800], 580 [61300], 435 [47200]$. **Fluorescence** (CH_2Cl_2): λ_{max} (nm) = 738 with $\lambda_{\text{ex}} = 560$; $\Phi_{\text{Fl}} = 0.19$.

Array org:

Under an argon atmosphere 87 mg (3.12×10^{-2} mmol, 1 equiv.) of compound **pcC**, 34 mg (6.24×10^{-2} mmol, 2 equiv.) of compound **oPMI** and 12 mg (6.24×10^{-2} mmol, 2 equiv.) of $\text{Zn}(\text{OAc})_2$ (H_2O -free) were heated in distilled quinoline (0.5 mL) at 165 °C for 15 h. The reaction mixture being cooled to room temperature and poured into 20 mL of 2N HCl and stirred for 30 min at 40 °C and adjusted to pH > 9 with NH_3 solution (25%). CH_2Cl_2 (40 mL) was added to the reaction mixture, the resulting two phases were separated, and the organic phase was washed with water and brine and dried over MgSO_4 . The crude product was purified first by column chromatography with CH_2Cl_2 /ethyl acetate 99:1 and successively by HPLC with CH_2Cl_2 (SiO_2 , normal phase) and precipitation from CH_2Cl_2 /methanol. Array **org** was obtained as a dark powder (51 mg, 1.54×10^{-2} mmol, yield 49%). $\text{C}_{217}\text{H}_{212}\text{N}_8\text{O}_{24}$ (3316.04). Mp > 400 °C. TLC: CH_2Cl_2 /ethyl acetate 99:1; $R_f = 0.49$. **$^1\text{H NMR}$** (400 MHz, CDCl_3 , 25 °C): δ (ppm) = 8.79 (bd, 2H, $^3\text{J} = 7.6$ Hz; Per-*H*); 8.69 – 8.65 (m, 6H; Per-*H*); 8.60 (s, 1H; Per-*H*); 8.53 – 8.50 (m, 2H; Per-*H*); 8.44 (d, 1H, $^3\text{J} = 8.0$ Hz; Per-*H*); 8.33 (bs, 4H; Per-*H*); 7.80 and 7.78 (each d, 2H, each $^3\text{J} = 8.0$ Hz; Per-*H*); 7.26 (bd, 8H; Phen-*H*); 7.12 and 7.11 (each s, 4H; Ar-*H*); 7.05 (s, 4H; Ar-*H*); 6.90 (bd, 8H, $^3\text{J} = 8.4$ Hz; Phen-*H*); 6.37 and 6.36 (each t, 4H, each $^3\text{J} = 7.5$ Hz; Ar-*H*); 6.24 and 6.17 (each bd, 8H; Ar-*H*); 5.29 – 5.23 and 5.20 – 5.13 (each m, 2H; N-*CH* and Cy-*H*); 4.53 – 4.47 (m, 8H; Ar- CH_2 -Ar); 4.11 – 4.05 (m, 8H; O- CH_2); 3.78 and 3.65 (bs and t, 12H; Pyrr-*H* and O- CH_2); 3.19 – 3.13 (m, 8H; Ar- CH_2 -Ar); 2.88 (bs, 4H; Pyrr-*H*); 2.66 – 2.57 (m, 2H; Cy-*H*); 2.29 – 2.24 (m, 2H; Alkyl-*H*); 2.09 – 1.76 (m, 31H; Pyrr-*H*, Propyl-*H*, Cy-*H*, Alkyl-*H*); 1.50 – 1.41 (m, 3H; Cy-*H*); 1.30 (bs, 48H; *tert*-Butyl-Phen-*H* und Alkyl-*H*); 1.11 (t, 12H, $^3\text{J} = 7.3$ Hz; Propyl-*H*); 0.92 – 0.82 (m, 18H; Propyl-*H* and Alkyl-*H*). **HR-MS** (ESI in CHCl_3 /acetonitrile): calcd for $\text{C}_{217}\text{H}_{220}\text{N}_{10}\text{O}_{24} [\text{M}+2\text{NH}_4]^{2+}$ (m/z) 1674.8151; found 1674.8146. **UV/vis** (CH_2Cl_2): λ (nm) $[\epsilon \text{ (M}^{-1}\text{cm}^{-1})] = 701 [46000], 580 [57100], 527 [116800], 489 [69800], 456 [43700], 435 [38000]$. **Fluorescence** (CH_2Cl_2): λ_{max} (nm) = 737 with $\lambda_{\text{ex}} = 490$; $\Phi_{\text{Fl}} = 0.16$.

Compound rc:

A suspension of 20 mg (3.24×10^{-2} mmol, 1 equiv.) of 5-monoamino-25,26,27,28-tetrakis(propoxy)-calix[4]arene, 38 mg (3.89×10^{-2} mmol, 1.2 equiv.) of **rPMI** and 61 mg (7.79×10^{-2} mmol, 2 equiv.) of $\text{Zn}(\text{OAc})_2$ (H_2O -free) was heated in 0.3 mL distilled quinoline at 165 °C for 10 h under an argon atmosphere. The reaction mixture being cooled to room temperature and poured into 2N HCl and stirred for 30 min at 40 °C. To the solution 50 mL of CH_2Cl_2 were added and the resulting organic phase was washed with water and brine and dried over MgSO_4 . The crude product was purified by column chromatography with CH_2Cl_2 /hexane 60:40 and 50:50, and successively by precipitation from CH_2Cl_2 /methanol. Compound **rc** was obtained as a red powder (21 mg, 1.29×10^{-5} mol, yield 40%). $\text{C}_{108}\text{H}_{112}\text{N}_2\text{O}_{12}$ (1630.05). Mp = 377 – 379 °C. TLC: CH_2Cl_2 /Hexan 60:40; R_f = 0.38. $^1\text{H NMR}$ (400 MHz, CDCl_3 , 25 °C): δ (ppm) = 8.28 and 8.25 (bs and s, 4H; Per-*H*); 7.26 – 7.20 (m, 4H; Phen-*H*); 7.09 (d, 2H, $^3J = 7.5$ Hz; Ar-*H*); 6.99 (s, 2H; Ar-*H*); 6.91 and 6.88 – 6.88 (t and m, 9H, $^3J = 7.4$ Hz; Phen-*H* and Ar-*H*); 6.24 (t, 2H, $^3J = 7.6$ Hz; Ar-*H*); 6.16 (dd, 2H, $^3J = 7.5$ Hz / $^4J = 1.0$ Hz; Ar-*H*); 6.07 (dd, 2H, $^3J = 7.5$ Hz / $^4J = 1.0$ Hz; Ar-*H*); 4.46 and 3.14 (AX, 4H, $^2J = 13.4$ and 13.6 Hz; Ar- CH_2 -Ar); 4.44 and 3.12 (AX, 4H, $^2J = 13.2$ and 13.5 Hz; Ar- CH_2 -Ar); 4.13 and 4.06 and 4.01 (each t, 6H, $^3J = 7.5$ and 8.3 and 8.2 Hz; N- CH_2 and O- CH_2); 3.69 – 3.60 (m, 8H; O- CH_2); 1.99 – 1.80 (m, 8H; Propyl-*H*); 1.71 – 1.63 (m, 2H; Butyl-*H*); 1.45 – 1.38 (m, 2H; Butyl-*H*); 1.30 and 1.28 (each s, 36H, *tert*-Butyl-Phen-*H*); 1.08 (t, 6H, $^3J = 7.5$ Hz; Propyl-*H*); 0.94 (t, 3H, $^3J = 7.5$ Hz; Propyl-*H*); 0.87 and 0.86 (each t, 6H, each $^3J = 7.5$ Hz; Propyl-*H*). **MS** (ESI in CHCl_3 /acetonitrile): calcd for $\text{C}_{108}\text{H}_{112}\text{N}_2\text{O}_{12}$ (m/z) 1628.82 $[\text{M}]^+$, $\text{C}_{108}\text{H}_{116}\text{N}_3\text{O}_{12}$ (m/z) 1646.86 $[\text{M}+\text{NH}_4]^+$, $\text{C}_{108}\text{H}_{112}\text{N}_2\text{O}_{12}\text{Na}$ (m/z) 1651.81 $[\text{M}+\text{Na}]^+$, and $\text{C}_{108}\text{H}_{112}\text{N}_2\text{O}_{12}\text{K}$ (m/z) 1667.79 $[\text{M}+\text{K}]^+$; found 1628.82, 1646.86, 1651.81, and 1667.79, respectively. **HR-MS** (ESI in CHCl_3 /acetonitrile): calcd for $\text{C}_{108}\text{H}_{112}\text{N}_2\text{O}_{12}$ (m/z) 1628.8215 $[\text{M}]^+$, $\text{C}_{108}\text{H}_{116}\text{N}_3\text{O}_{12}$ (m/z) 1646.8558 $[\text{M}+\text{NH}_4]^+$, and $\text{C}_{108}\text{H}_{112}\text{N}_2\text{O}_{12}\text{Na}$ (m/z) 1651.8113 $[\text{M}+\text{Na}]^+$; found 1628.8210, 1646.8554, and 1651.8108, respectively. **Analysis**: calcd (%) for $\text{C}_{112}\text{H}_{116}\text{N}_4\text{O}_{12}$ (1710.14): C 78.66; H 6.84; N 3.28; found: C 78.58; H 6.91; N 3.34. **UV/vis** (CH_2Cl_2): λ (nm) [ϵ ($\text{M}^{-1}\text{cm}^{-1}$)] = 578 [47400]. **Fluorescence** (CH_2Cl_2): λ_{max} (nm) = 608; Φ_{Fl} = 0.80.

¹H NMR Spectra.

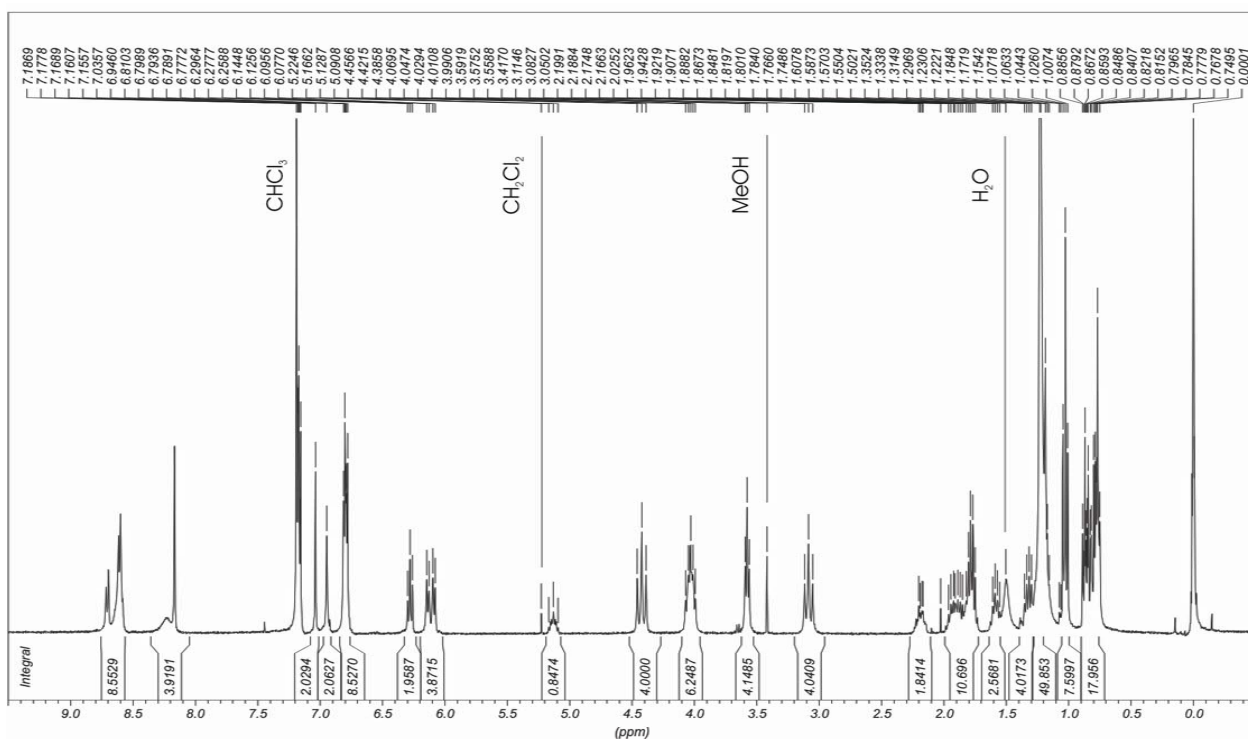


Figure S1. ¹H NMR spectrum (400 MHz, CDCl₃, 25 °C) of array or.

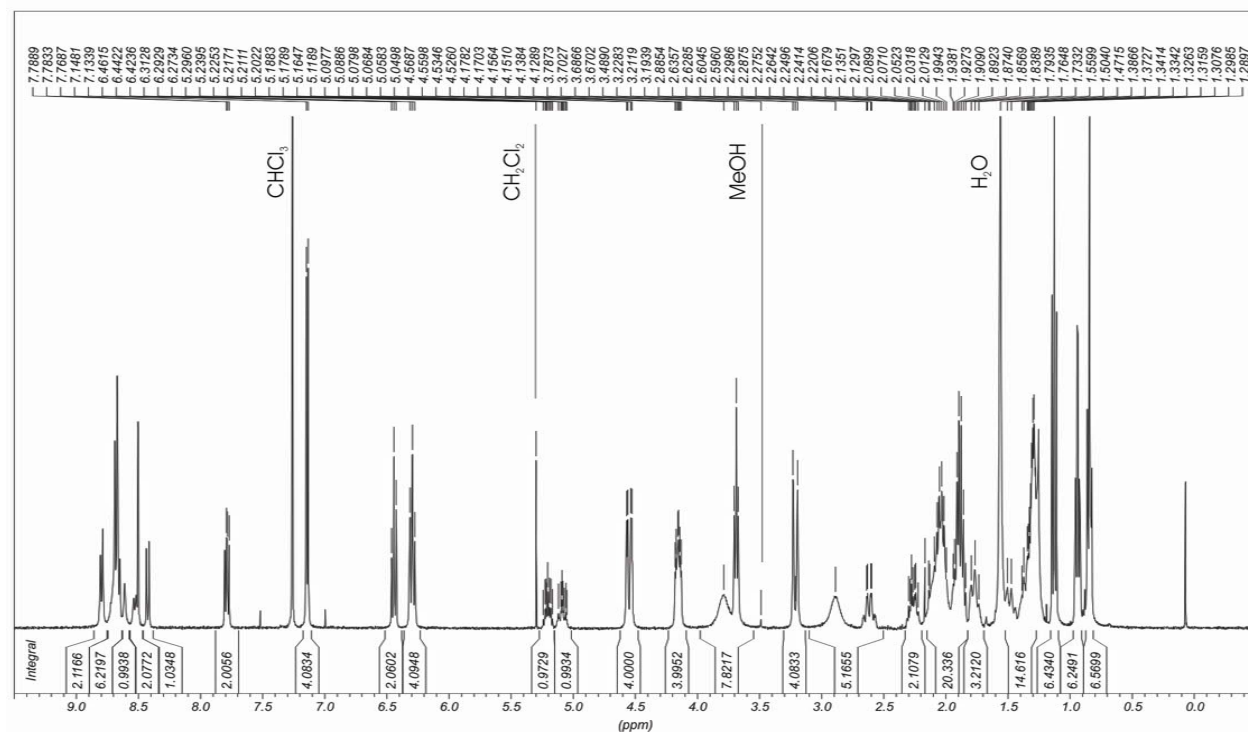


Figure S2. ¹H NMR spectrum (400 MHz, CDCl₃, 25 °C) of array og.

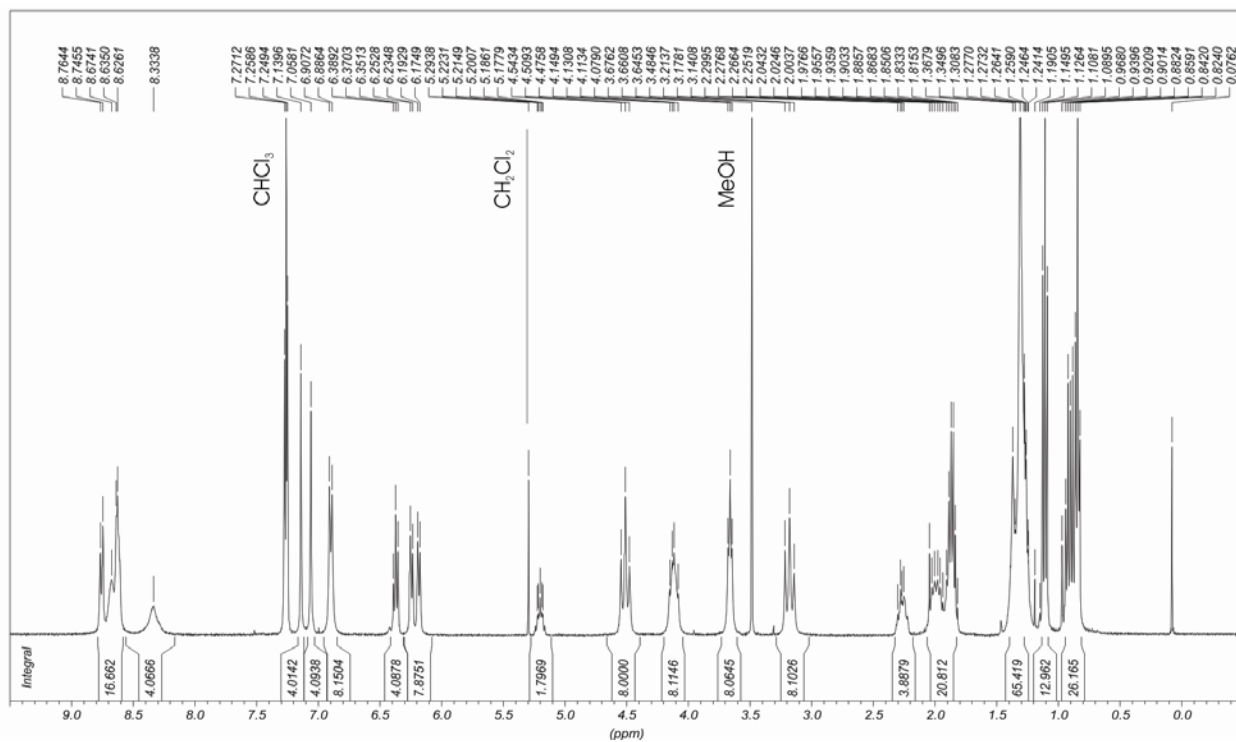


Figure S3. ¹H NMR spectrum (400 MHz, CDCl₃, 25 °C) of array **oro**.

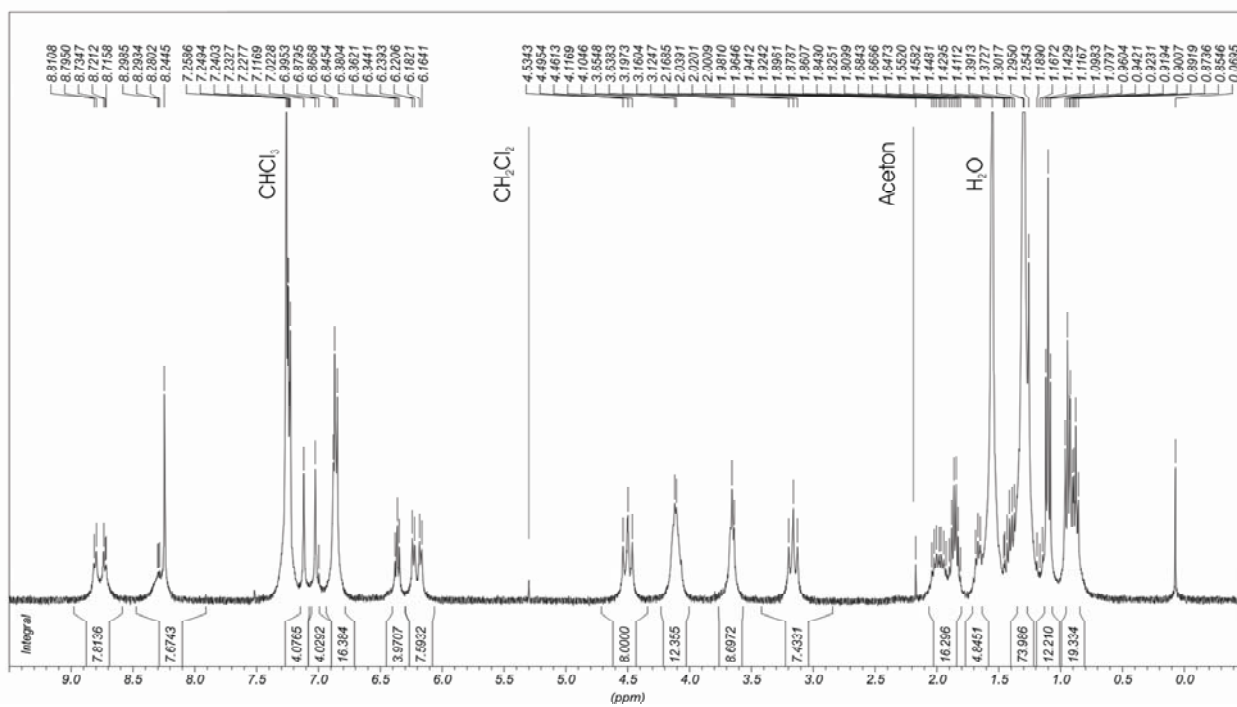


Figure S4. ¹H NMR spectrum (400 MHz, CDCl₃, 25 °C) of array **ror**.

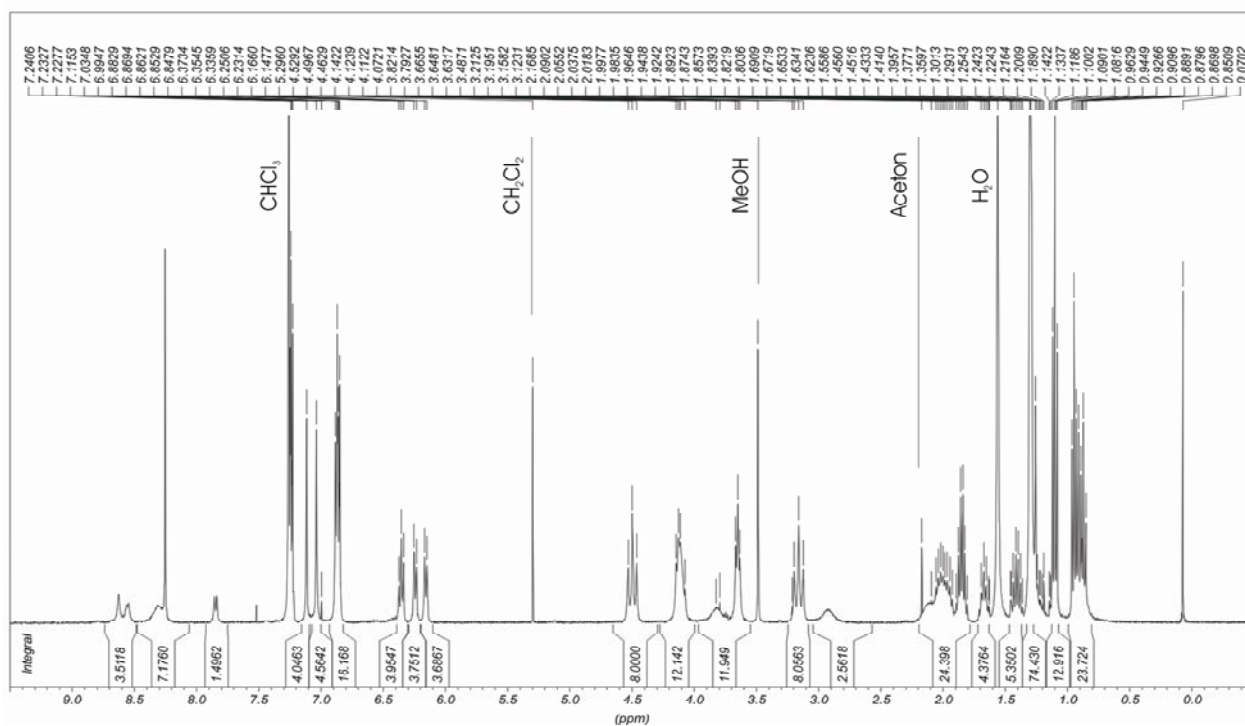


Figure S5. ¹H NMR spectrum (400 MHz, CDCl₃, 25 °C) of array rgr.

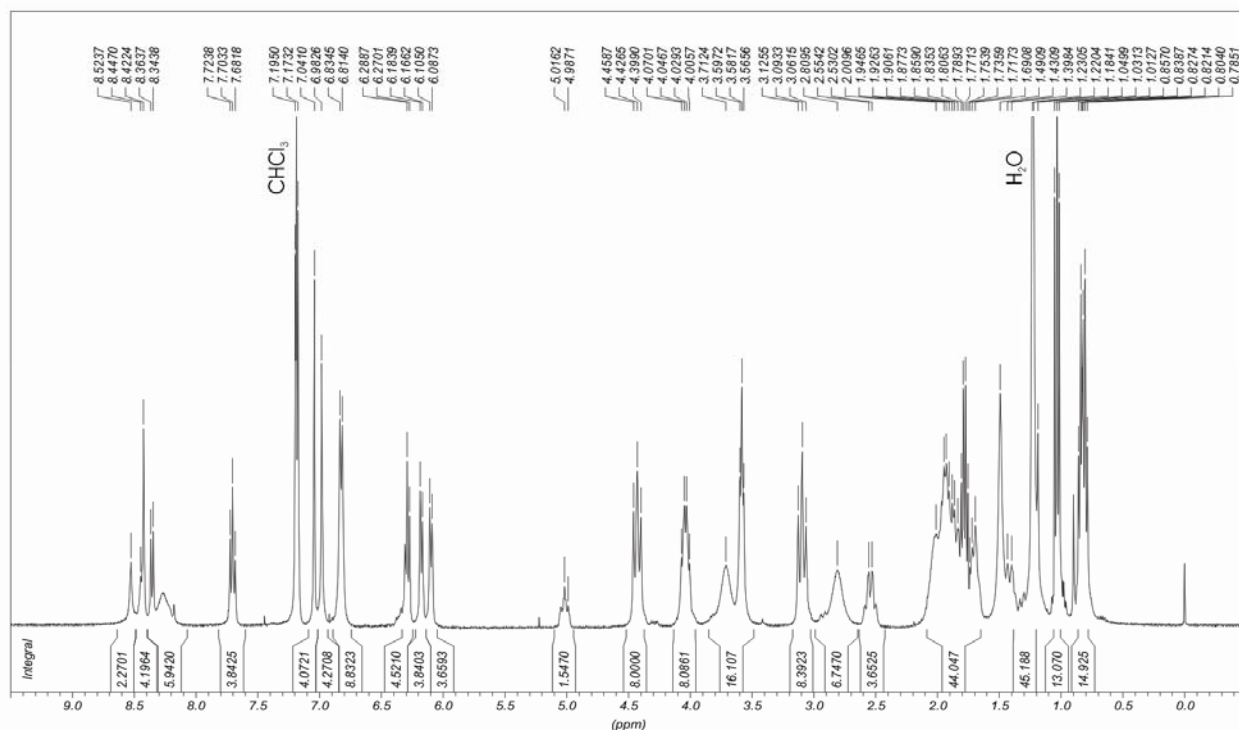


Figure S6. ¹H NMR spectrum (400 MHz, CDCl₃, 25 °C) of array grg.

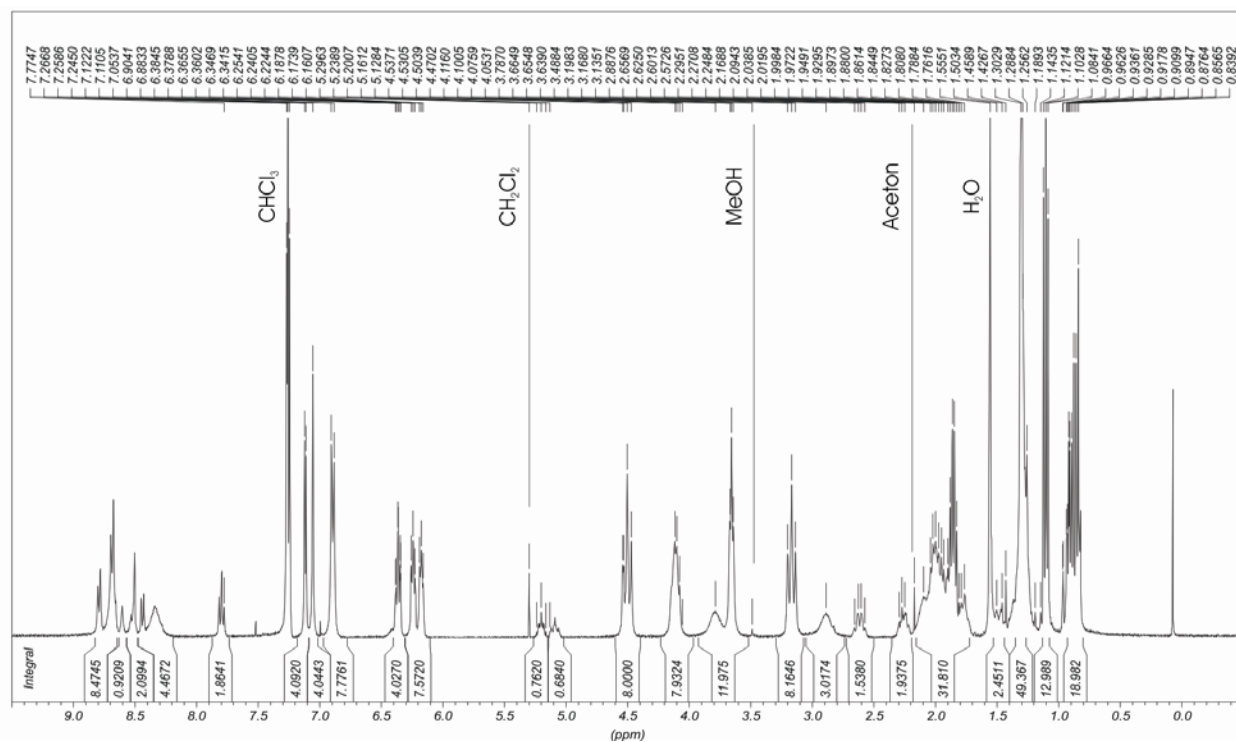


Figure S7. ¹H NMR spectrum (400 MHz, CDCl₃, 25 °C) of array org.

Molecular Modeling.

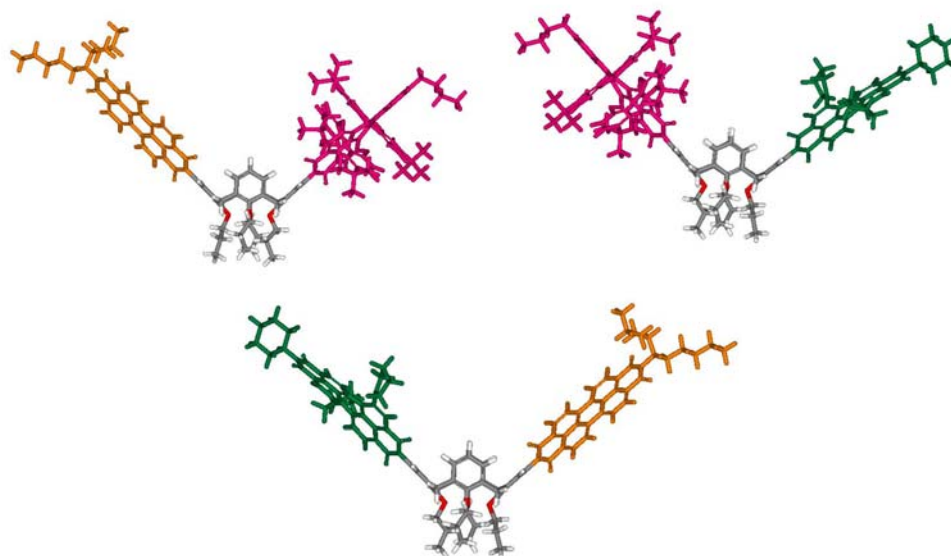


Figure S8. Side views of molecular structures obtained from geometry optimizations (force field, Macromodel 8.0, potential MMFF) of PBI – calix[4]arene arrays. Top (left): array **or**; top (right): array **rg**. Bottom: array **og**. PBI chromophores are given in respective color (orange, red, and green, respectively) for clarity.

Temperature-Dependent ^1H NMR Studies.

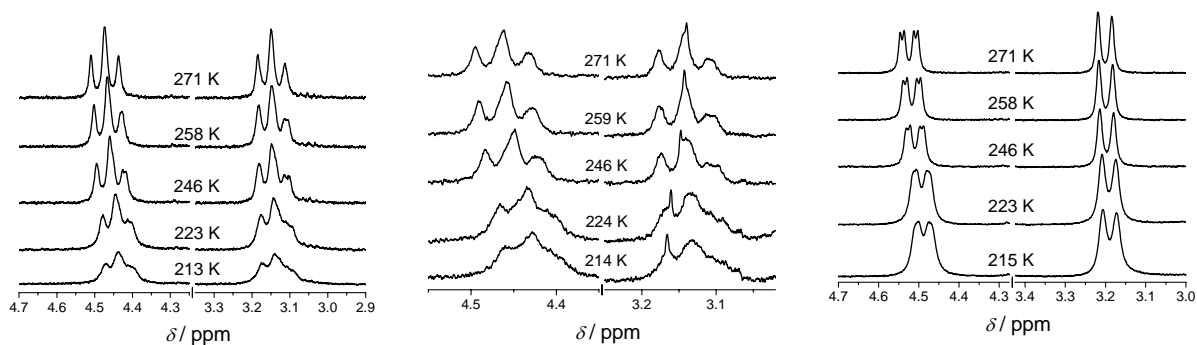


Figure S9. Sections of variable temperature ^1H NMR spectra (400 MHz, in CDCl_3) of arrays **or** (left), **rg** (middle), and **og** (right) showing the Ar- CH_2 -Ar protons of the respective calix[4]arene moiety. Temperatures are indicated above the spectra.

Optical Spectra.

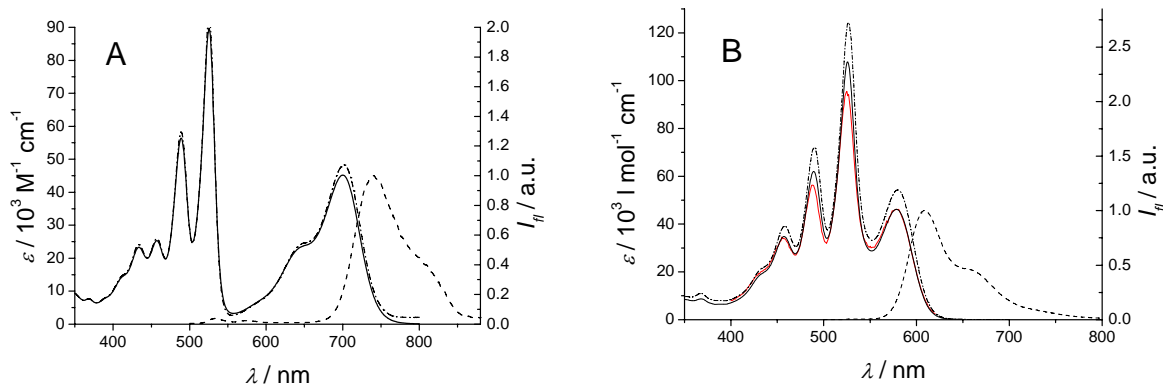


Figure S10. (A) UV/vis absorption (black, solid line), calculated UV/vis absorption (black, dash-dotted line, from $\epsilon(\mathbf{oc}) + \epsilon(\mathbf{gc})$), and fluorescence emission spectra (black, dashed line; $\lambda_{\text{ex}} = 490$ nm) of array **og** in CH_2Cl_2 . (B) UV/vis absorption (black, solid line), calculated UV/vis absorption (black, dash-dotted line; from $\epsilon(\mathbf{oc}) + \epsilon(\mathbf{rc})$), fluorescence emission (black, dashed line; $\lambda_{\text{ex}} = 490$ nm), and fluorescence excitation spectra (red, solid line; $\lambda_{\text{det}} = 700$ nm) of array **or** in CH_2Cl_2 .

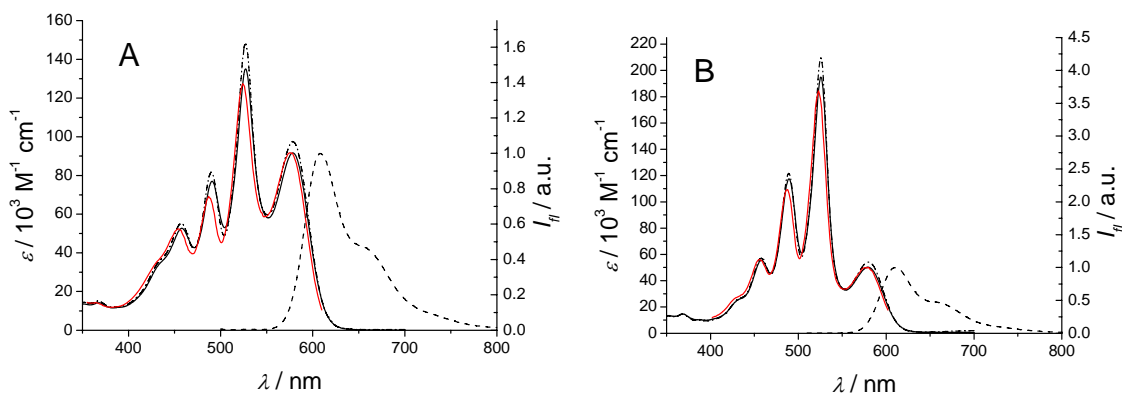


Figure S11. (A) UV/vis absorption (black, solid line), calculated UV/vis absorption (black, dash-dotted line; from $\epsilon(\mathbf{oc}) + 2x \epsilon(\mathbf{rc})$), fluorescence emission (black, dashed line; $\lambda_{\text{ex}} = 490$ nm), and fluorescence excitation spectra (red, solid line; $\lambda_{\text{det}} = 700$ nm) of array **ror** in CH_2Cl_2 . (B) UV/vis absorption (black, solid line), calculated UV/vis absorption (black, dash-dotted line; from $\epsilon(\mathbf{rc}) + 2x \epsilon(\mathbf{oc})$), fluorescence emission (black, dashed line; $\lambda_{\text{ex}} = 490$ nm), and fluorescence excitation spectra (red, solid line; $\lambda_{\text{det}} = 700$ nm) of array **oro** in CH_2Cl_2 .

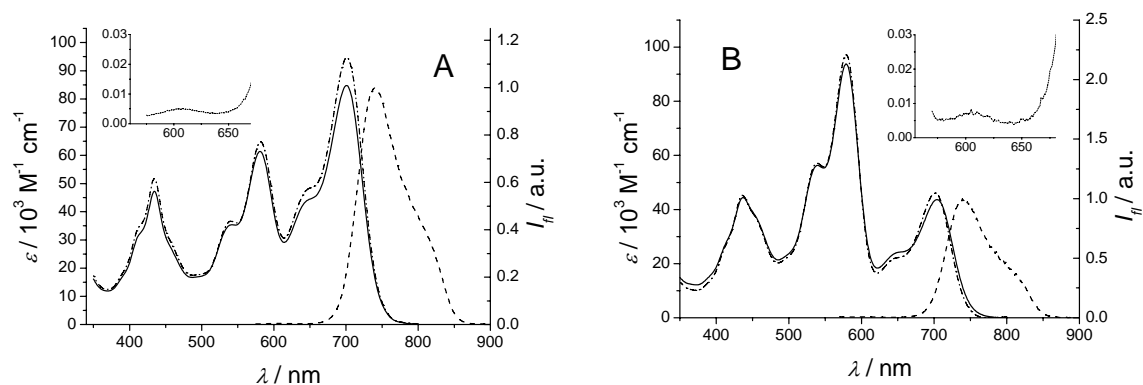


Figure S12. (A) UV/vis absorption (black, solid line), calculated UV/vis absorption (black, dash-dotted line; from $\epsilon(\mathbf{rc}) + 2x \epsilon(\mathbf{gc})$), and fluorescence emission spectra (black, dashed line; $\lambda_{\text{ex}} = 560 \text{ nm}$) of array **grg** in CH_2Cl_2 . Inset: Magnification of fluorescence emission spectrum in the range of 560 to 670 nm. (B) UV/vis absorption (black, solid line), calculated UV/vis absorption (black, dash-dotted line; from $\epsilon(\mathbf{ge}) + 2x \epsilon(\mathbf{rc})$), and fluorescence emission spectra (black, dashed line; $\lambda_{\text{ex}} = 560 \text{ nm}$) of array **rgr** in CH_2Cl_2 . Inset: Magnification of fluorescence emission spectrum in the range of 550 to 680 nm.

Femtosecond Transient Absorption Spectra in CH₂Cl₂.

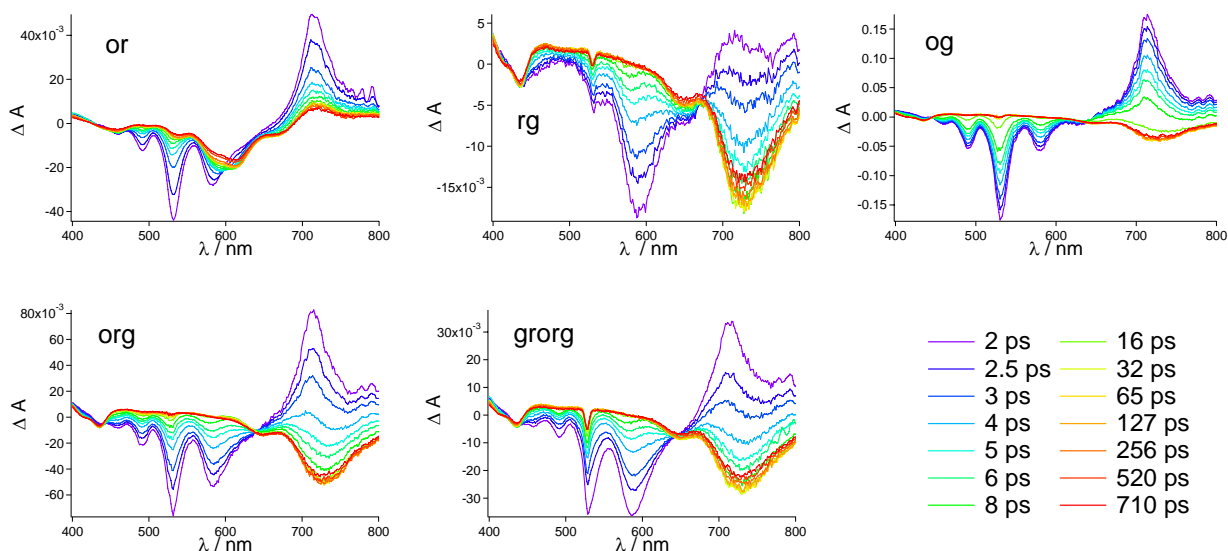


Figure S13. Femtosecond transient absorption spectra and corresponding time delays in CH₂Cl₂ after photoexcitation at 530 nm. Top: arrays **or** (left), **rg** (middle), and **og** (right). Bottom: arrays **org** (left) and **grorg** (middle). Spectra of array **org** are also shown here for comparison. The scattered laser pulse is observed for arrays **rg** and **grorg**.

Upon photoexcitation of array **or** the instantaneous development of strong negative signals at 490, 530, and 580 nm is observed together with a broad positive absorption band centered at 715 nm. The latter features are typical for excited state transitions of the *orange* perylene bisimide (PBI) chromophore, whilst the bands at 490 nm and 530 nm indicate ground state bleaching and stimulated emission (at 580 nm).^{S12} The amplitudes of the negative signals decrease and shift toward a negative signal at 590 nm which was assigned to the ground state bleaching of the *red* PBI chromophore.^{S13} Within the time frame of the experiment, the negative band at 590 nm slightly shifts the position of its maximum to 610 nm which might be attributed to conformational changes of the red PBI.^{S14} Furthermore, the sharp positive band at 715 nm (excited state absorption of the orange PBI) decreases with a similar rate and converts to a low intensity broader feature that is attributed to the absorption of the excited state of the red PBI. No recovery of the ground state was observed within the instrument's time frame of 1 ns, which is plausible because the excited-state lifetime of the red PBI chromophore is in the nanosecond time regime. These findings indicate the depopulation of the singlet excited state of the orange PBI and, therefore, provide evidence for the energy transfer from the *orange* to the *red* PBI unit as already observed by steady-state emission spectroscopy. Similar band shapes and positions as well as an identical spectral evolution are also

present in the femtosecond transient absorption spectra obtained for arrays **oro** and **ror** (see Figure S14).

The photoexcitation of array **rg** leads to the immediate formation of transient absorption signals at 435 and 588 nm (negative) as well as at 715 nm (positive). These spectral features are inherent to the singlet excited state absorption of the *red* PBI unit^{S13} which decays very rapidly to form a long-lived bleach band centered at 730 nm, together with a small negative absorption pattern at 435 nm. A weak broad positive absorption between 450 and 600 nm is also present. These spectral patterns are typical for the optically excited *green* PBI chromophore.^{S14} Such bands clearly confirm the fast energy transfer from the *red* (here: energy donor) to the *green* PBI (here: energy acceptor) chromophoric units. Similar band shape and position as well as an identical spectral evolution are also present in the femtosecond transient absorption spectra obtained for arrays **rgr** and **grg** (see Figure S14). For both arrays, no conformational effect of the red PBI is observed, probably due to its very fast decay (see above).

Intense negative signals are present in the femtosecond transient absorption spectra of array **og** at 490, 530, and 580 nm which can be assigned to the combined signals of ground state bleaching and stimulated emission of the *orange* PBI chromophore.^{S12} These features are accompanied by a strong positive absorption band with a maximum centered at 715 nm that is indicative for the singlet excited state absorption of the *orange* PBI chromophore. These spectral patterns decay very rapidly, but concomitantly give rise to a long-lived negative signal at around 730 nm together with a negative feature at 435 nm of very weak intensity. The latter can be attributed to the formation of the excited singlet state of the *green* PBI unit,^{S14} and thus provide convincing evidence for the energy transfer between the *orange* and the *green* chromophoric units. However, the amplitude for the bleaching of the green PBI chromophore at 730 nm remains rather small (compared with that of array **rg**) due to the formation of radical anions of the orange PBI unit (that absorbs at about 700 nm)^{S8} by the competing PET process from the electron-rich calix[4]arene to the electron-poor orange PBI.

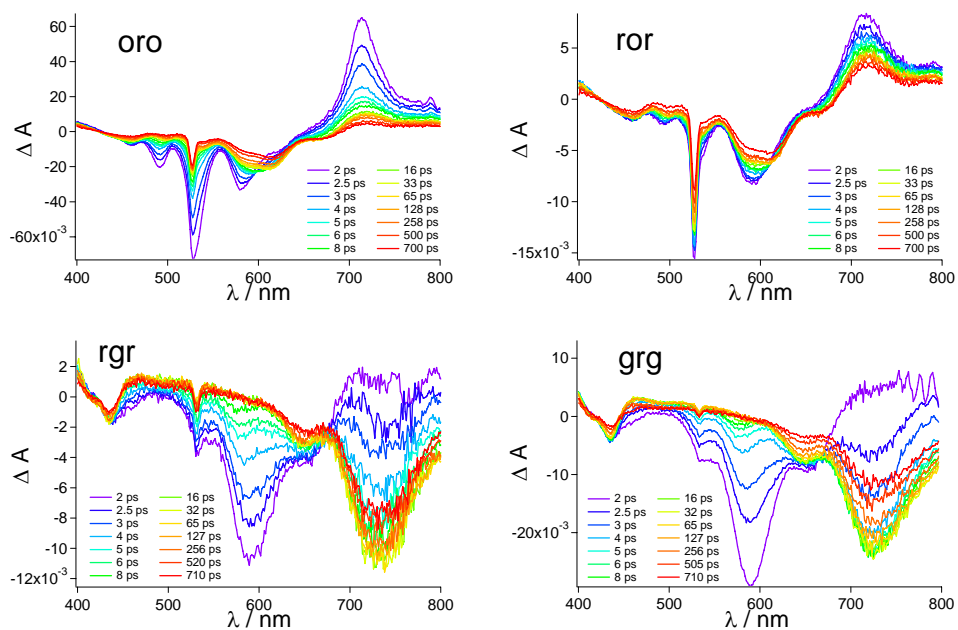


Figure S14. Femtosecond transient absorption spectra and corresponding time delays in CH_2Cl_2 after photoexcitation at 530 nm. Top: arrays **oro** (left) and **ror** (right). Bottom: arrays **rgr** (left) and **grg** (right). The scattered laser-pulse is observed for arrays **oro**, **ror**, and **rgr**.

Femtosecond Transient Absorption Spectra in Toluene and Benzonitrile.

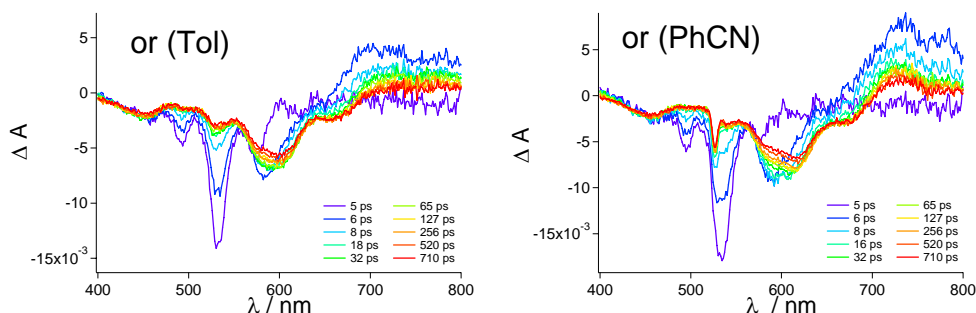


Figure S15. Femtosecond transient absorption spectra and corresponding time delays after photoexcitation at 530 nm for array **or**. Left: in toluene (Tol); right: in benzonitrile (PhCN). The scattered laser-pulse is observed for the measurement in benzonitrile.

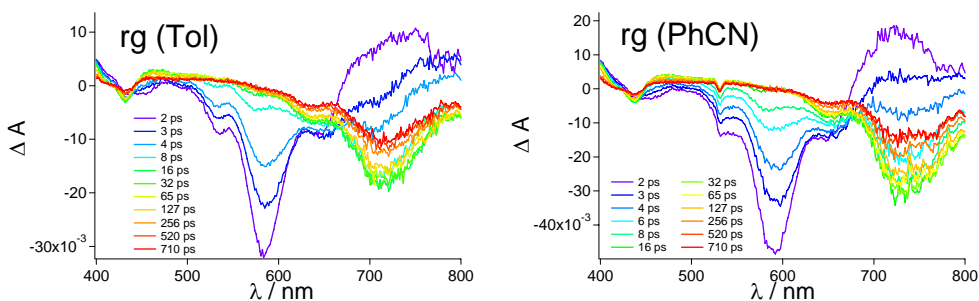


Figure S16. Femtosecond transient absorption spectra and corresponding time delays after photo-excitation at 530 nm for array **rg**. Left: in toluene (Tol); right: in benzonitrile (PhCN). The scattered laser-pulse is observed for the measurement in benzonitrile.

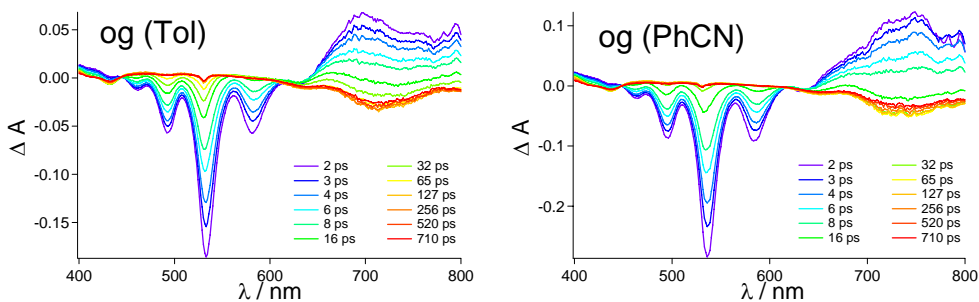


Figure S17. Femtosecond transient absorption spectra and corresponding time delays after photoexcitation at 530 nm for array **og**. Left: in toluene (Tol); right: in benzonitrile (PhCN).

Representative Time-Resolved Traces in CH₂Cl₂.

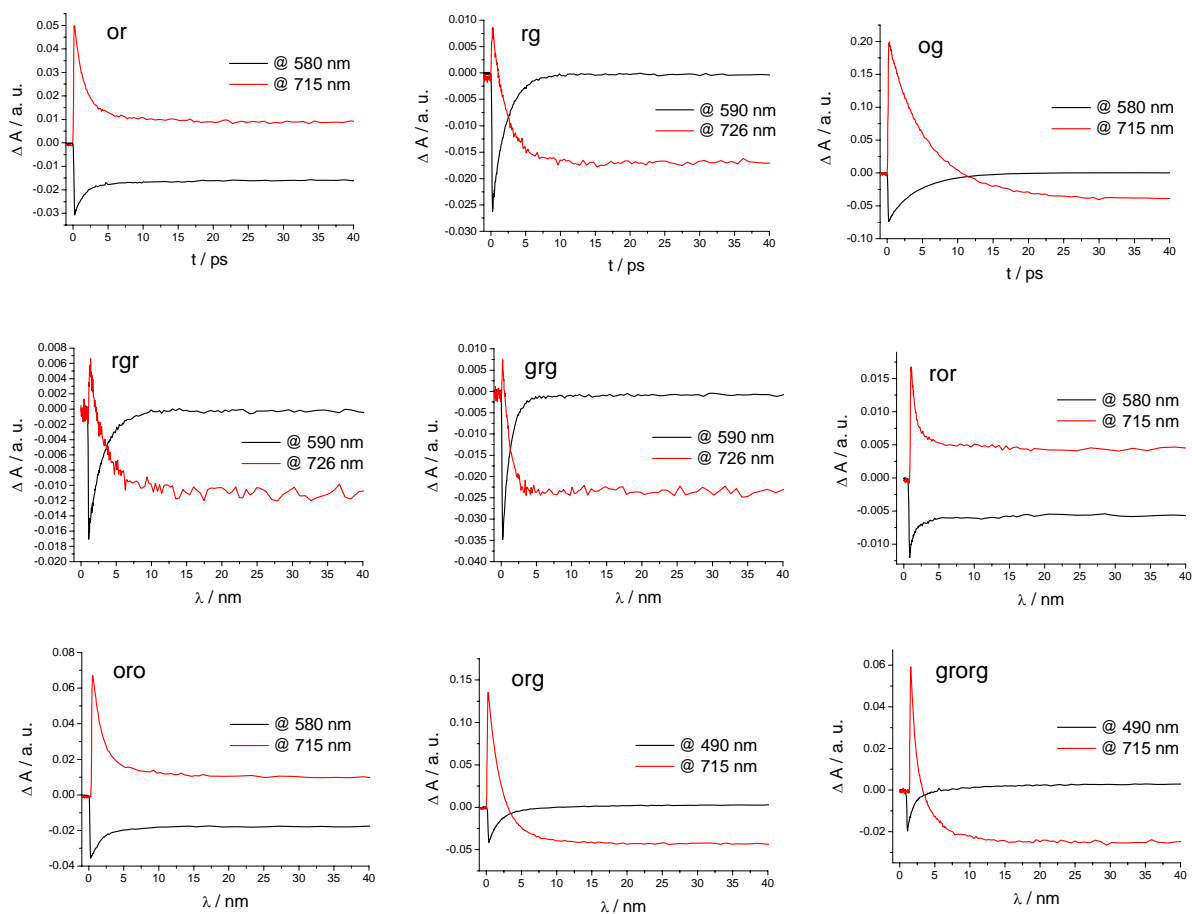


Figure S18. Kinetic profiles of the transient absorption in CH₂Cl₂. Top: array **or** (left) measured at 580 nm (black line) and 715 nm (red line); array **rg** (middle) measured at 590 nm (black line) and 726 nm (red line); array **og** (right) measured at 580 nm (black line) and 715 nm (red line). Middle: array **rgr** (right) measured at 590 nm (black line) and 726 nm (red line); array **grg** (middle) measured at 590 nm (black line) and 726 nm (red line); array **ror** (right) measured at 580 nm (black line) and 715 nm (red line). Bottom: array **oro** (left) measured at 580 nm (black line) and 715 nm (red line), array **org** (middle) measured at 490 nm (black line) and 715 nm (red line), array **gorg** (right) measured at 490 nm (black line) and 715 nm (red line). Kinetic profiles of array **org** are also shown here for comparison.

Representative Time-Resolved Traces in Toluene and Benzonitrile.

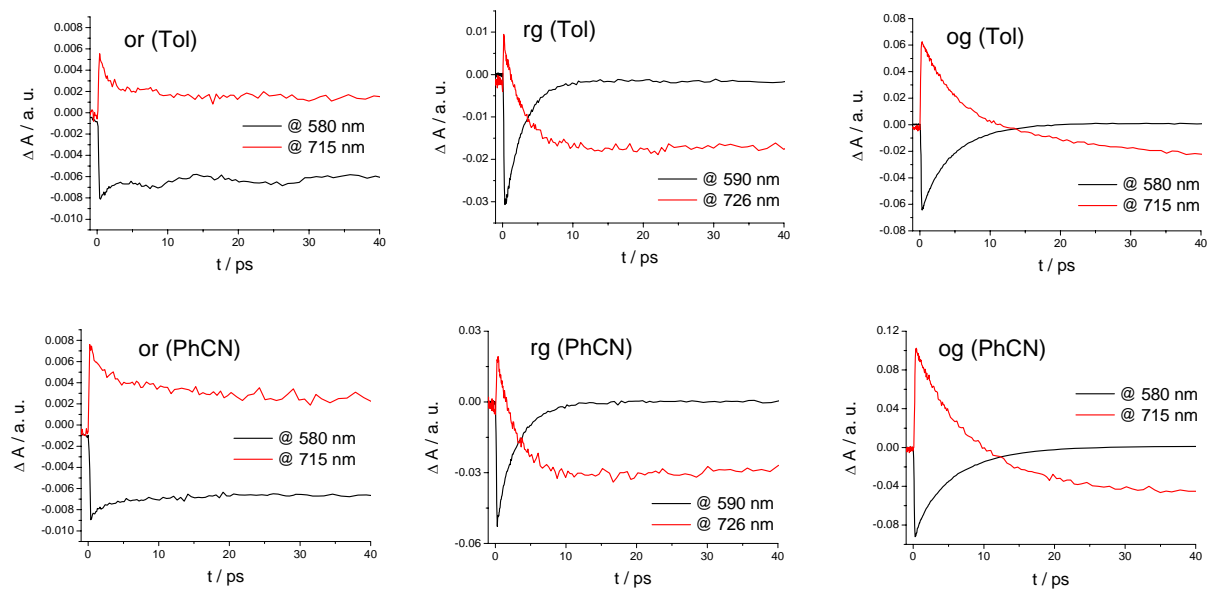


Figure S19. Kinetic profiles of the transient absorption: (top) in toluene (Tol) and (bottom) in benzonitrile (PhCN). Top (left): array **or**, measured at 580 nm (black line) and 715 nm (red line); top (middle): array **rg**, measured at 590 nm (black line) and 726 nm (red line); top (right): array **og**, measured at 580 nm (black line) and 715 nm (red line). Bottom (left): array **or**, measured at 580 nm (black line) and 715 nm (red line); bottom (middle): array **rg**, measured at 590 nm (black line) and 726 nm (red line); bottom (right): array **og**, measured at 580 nm (black line) and 715 nm (red line).

Details on Global and Target Analysis.

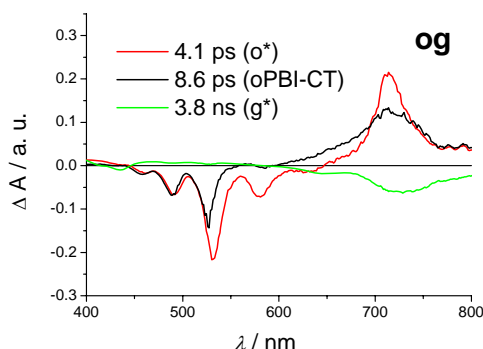


Figure S20. Species-associated difference spectra (SADS) resulting from the target analysis of the femtosecond transient absorption data employing the kinetic schemes depicted in Figure 7 and Figure S22, respectively. Shown are processes after photoexcitation at 530 nm with the species: o* (red line), oPBI-CT (black line), and g* (green line). Features due to Raman scattering and fast solvent reorganization processes were omitted for clarity.

For array **og**, the initial spectrum in Figure S20 (red line) shows the transient absorption features of the orange PBI chromophore^{S8} and was accordingly assigned to the excited singlet state of the orange PBI. This SADS changes within 4.1 ps into *two* following states (represented by black and green line in Figure S20) as a second deactivation route via the charge transfer state was included into the model.^{S8} The major deactivation pathway (62%) which relates to the energy transfer to the green chromophore is represented by the final green SADS in Figure S20; this state is populated within 6.7 ps. The related rate constant k_{ET} for the energy transfer between the *orange* and the *green* donor-acceptor pair can be afforded from the respective reciprocal value, giving a rate constant of $k_{ET} = 1.5 \times 10^{11} \text{ s}^{-1}$. The obtained green SADS decays with a lifetime of 3.8 ns and its spectral features can be clearly assigned to the excited state of the green chromophore, referred to as g*. Thus, an efficient energy transfer from the *orange* to the *green* chromophore is evident. However, it has to be noted that the longest lifetime values are prone to large errors due to the time frame of the instrument of 1 ns and, therefore, differ from the values obtained from time-resolved emission experiments.^{S7,S8} They, however, reveal the correct order of magnitude of the lifetimes of the reference chromophores and represent their lower limits. The second competitive deactivation pathway (38%) of the excited state of the orange PBI o* (black line in Figure 6) relates to the formation of the CT state of the calix[4]arene-orange PBI subunit and is represented by the black SADS; this state is populated within 10.8 ps. The related rate constant k_{CT} can be obtained from the reciprocal value of τ_{CT} and is found to be $k_{CT} = 0.92 \times 10^{11} \text{ s}^{-1}$. The black curve decays with a

lifetime of 8.6 ps and exactly reveals the spectral features of a charge transfer state as the stimulated emission at 580 nm is not observed any longer and the band at around 700 nm is significantly broadened. From this clear spectral evidence, the formation of a charge-separated state involving the formation of the orange PBI monoanion can be concluded. A similar competitive pathway via formation of a CT state of the calix[4]arene-PBI subunit was already observed for the orange reference compound **oc**.^{S8}

Table S1. Rate constants in CH₂Cl₂ obtained from the global and target analysis of the experimental data employing the model depicted in Figure 7

Cmpd	rate constant k (10^{11} s^{-1}) ^a				
	ET $\text{o}^* \rightarrow \text{r}^*$	ET $\text{r}^* \rightarrow \text{g}^*$	ET $\text{o}^* \rightarrow \text{g}^*$	CT to $(\text{oPBI})^{\bullet-}$	$(\text{oPBI})^{\bullet-}$
or	6.4			1.2	1.5
oro	6.3			1.34	1.5
ror	12.6			3.3	1.8
rg		4.0			
rgr		3.9			
grg		8.5			
org	7.1	3.9		1.0	0.95
grorg	15.8	3.4		2.2	1.1
og			1.5	0.92	1.2
oc ^b				0.40	1.7
oref				0.00	0.00

^a Relative precision of the rates is 10%. ^b See ref. 8.

In order to resolve the individual contributions from the respective excited state species, a simultaneous target analysis of the femtosecond transient data of arrays **og** and **org** has been applied using the kinetic scheme depicted in Figure 7 and Figure S22, respectively. Note that the SADS shown in Figure 6 are perfectly consistent with the SADS of o^* , $(\text{oPBI})^{\bullet-}$ and g^* shown in Figure S20, and that the r^* SADS (red line in Figure 6) displays the expected features: bleaching at 540 nm, bleaching plus stimulated emission at 590 nm, and a broad excited state absorption above 700 nm. The selected traces depicted in Figure S21 highlight the important processes: At 610 nm the initial bleaching plus stimulated emission is larger in array **org** (black line) than in array **og** (red line) due to the direct excitation of r^* . The energy transfer from o^* to r^* is visible as an increase of the black line up to about 0.7 ps, after which it starts to decrease due to energy transfer to g^* . At 485 nm bleaching of **o** is monitored. The red line is larger because exclusively o^* is excited in **og**. The bleaching of **o** decays partly with 8 ps due to the $(\text{oPBI})^{\bullet-}$, which is more abundant in

compound **og**. But the main decay of o^* is due to energy transfer, which is much faster in array **org** than in **og**. At 725 nm all states contribute. Here the increased energy transfer efficiency can directly be observed: at late times the black negative curve from **org** is about 30% larger than the red negative curve from array **og**, consistent with an efficiency increase from 62% to 89% (vide infra).

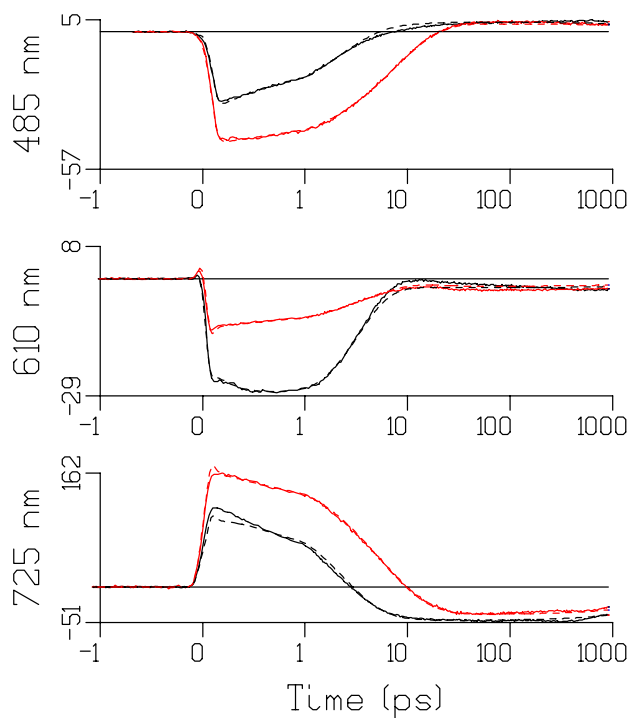


Figure S21. Selected traces and fits (dashed lines) of transient absorption of arrays **og** (red) and **org** (black) in CH_2Cl_2 . The decay of the ground state bleaching of o measured at 485 nm, the rise and decay time of the bleaching of the r^* state measured at 610 nm, and the concomitant decay of o^* , and o^* and $r^* S_1 \rightarrow S_n$ absorption, rise and decay of the o CT state, and rise of g^* stimulated emission at 725 nm. Note that the time axis is linear up to 1 ps, and logarithmic thereafter.

Gibbs Free Energy for Photoinduced Electron Transfer.

To examine the feasibility of a photoinduced charge separation, the Gibbs free energy of an intramolecular charge-separated state (ΔG_{CS}) was calculated for compound **rc** using the following equation (see also: Weller, A. Z. *Phys. Chem.* 1982, 133, 93–98. For details on a similar calculation for compound **oc**, see ref. S8):

$$\Delta G_{CS} = e[E_{ox}(D) - E_{red}(A)] - E_{00} - \frac{e^2}{4\pi\epsilon_0\epsilon_S R_{CC}} - \frac{e^2}{8\pi\epsilon_0} \left(\frac{1}{r^+} + \frac{1}{r^-} \right) \left(\frac{1}{\epsilon_{ref}} - \frac{1}{\epsilon_S} \right)$$

For the calculation of ΔG_{CS} , the respective first reduction potential $E_{red}(A) = -1.20$ V of compound **rc** and the oxidation potential of the calix[4]arene moiety of $E_{ox}(D) = +1.12$ V were used (both values obtained in CH_2Cl_2 and calibrated vs ferrocene/ferrocenium; for details see ref. S8). The distance between the centers of the donor and acceptor segment R_{CC} were estimated to $R_{CC} = 8.61$ Å (from an energy minimized modeling structure). Substitution of all remaining parameters (with ϵ_{ref} being equal to ϵ_S , the last solvent-related term in the equation vanishes) shows that the intramolecular charge-separated state in CH_2Cl_2 is higher in energy than the respective singlet excited state for compound **rc** ($E_{00} = 2.07$ eV; calculated from the intersection of the normalized absorption and fluorescence spectra). Accordingly, the electron transfer in CH_2Cl_2 from the calix[4]arene substituent to the perylene bisimide moiety for compound **rc** is a slightly *endergonic* process ($\Delta G_{CS} = +0.063$ eV). Therefore, it can be assumed that the formation of a charge-separated state consisting of the radical cation of the calix[4]arene moiety and the radical anion of the red perylene bisimide unit is energetically not feasible.

Energy Level Diagrams.

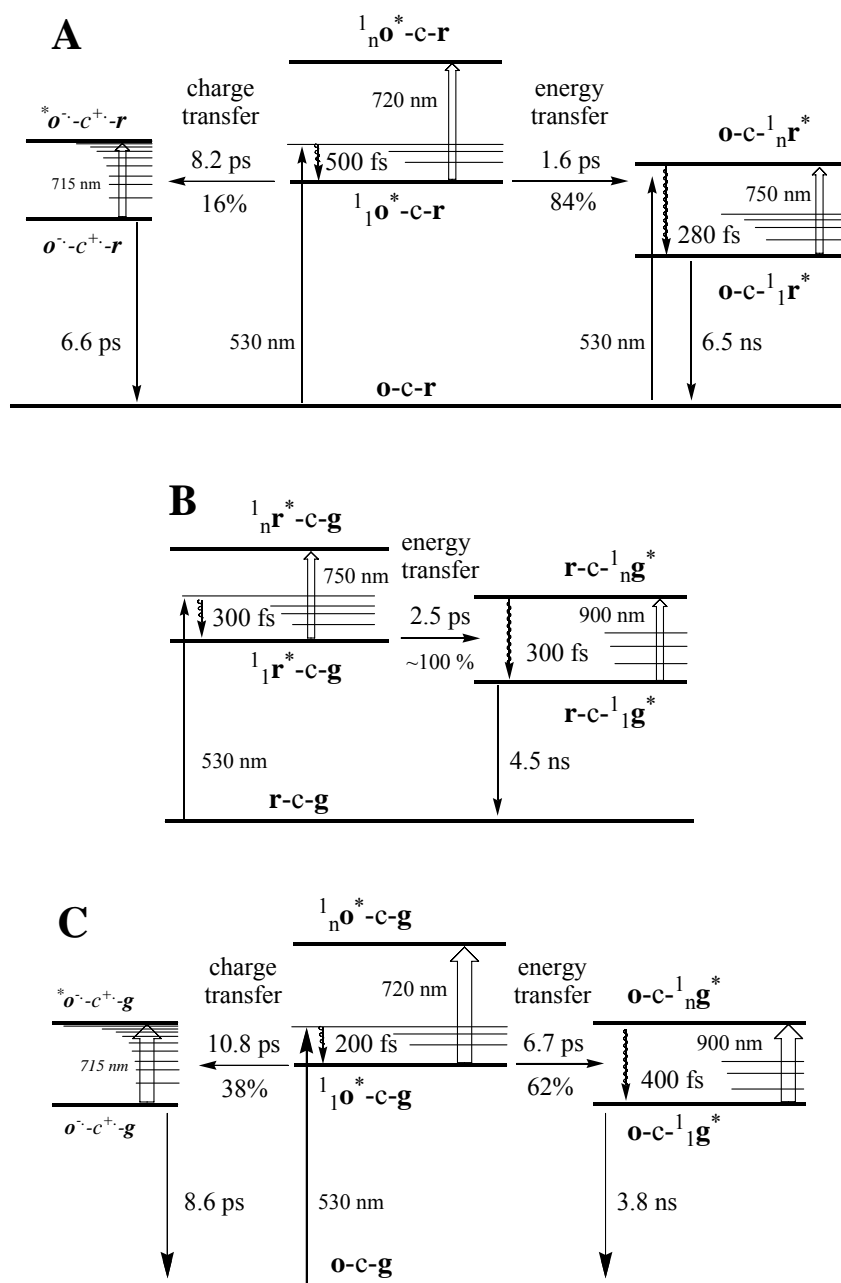


Figure S22. Energy level diagrams showing energy and electron transfer pathways in CH_2Cl_2 obtained with global and target analysis, together with the main decay times corresponding to the respective states: (A) for array **or**, (B) for array **rg**, and (C) for array **og**. Note that lifetimes in the ns time range are less reliable due to the 1ns time frame of the experiment and thus represent lower limits.

Details on Femtosecond Transient Absorption Data in Toluene and Benzonitrile.

The impact of the solvent polarity on the transient absorption spectra and the energy transfer rates has been studied for the three systems **or**, **rg**, and **og**. For this purpose, the less polar solvent toluene ($\epsilon_r = 2.4$) and the more polar solvent benzonitrile ($\epsilon_r = 25.9$) were applied. The obtained femtosecond transient absorption data as well as representative kinetic traces are shown in Figures S15-S17 and S19, and the lifetime values obtained from the global and target analysis are summarized in Table S2. As expected, the energy transfer rates and the kinetic profiles only differ slightly in solvents of different polarity. For the energy transfer rate from the *orange* to the *red* PBI unit in array **or** in both toluene and benzonitrile, a rate constant of 1.6 ps was obtained, respectively. Likewise, energy transfer rates from the *red* to the *green* PBI unit for array **rg** in toluene of 2.7 ps and in benzonitrile of 2.9 ps were obtained. Similarly, also for the energy transfer rates from the orange to the green PBI unit for compound **og** rates of 7.4 ps and 8.1 ps were obtained in toluene and benzonitrile, respectively. This behavior is in agreement with the solvent independency normally observed for Förster-type resonance energy transfer.^{S15} Remarkably, also the rates of charge separation remain almost constant in these two solvents for arrays **or** and **og**. In contrast, the charge recombination kinetics show a clear solvent dependency. For array **or** in toluene, a value for the recombination of the CT state of the calix[4]arene-PBI subunit of 25 ps is found which is significantly reduced for the more polar solvents CH₂Cl₂ and benzonitrile (see Table S2) and likewise, for array **og**, similar trends for the charge recombination are observed. This behavior can be attributed to Marcus inverted region effects as have already been observed for compound **oc**^{S8} and for other electron donor-acceptor systems.^{S16}

Lifetimes from Global and Target Analysis in Toluene and Benzonitrile.

Table S2. Selected lifetimes in toluene (Tol), CH₂Cl₂, and benzonitrile (PhCN) obtained from the global and target analysis of the experimental data

Cmpd	solv.	lifetime τ (ps) ^a						
		ET o*→r*	ET r*→g*	ET o*→g*	CT to (oPBI) ⁻	(oPBI) ⁻	r*→r	g*→g
or (Tol)	0.3	1.6			11.0	25.0	5000	
or (CH ₂ Cl ₂)	0.2	1.6			8.0	6.7	5000	
or (PhCN)	0.3	1.6			15.0	7.5	5200	
rg (Tol)	0.1		2.7					2000
rg (CH ₂ Cl ₂)	0.3		2.5					3300
rg (PhCN)	0.1		2.9					2400
og (Tol)	0.1			7.4	14.0	35.0		2200
og (CH ₂ Cl ₂)	0.2			6.7	10.8	8.6		3800
og (PhCN)	0.3			8.1	15.0	9.8		1400

^a Relative precision of the lifetimes and rates is 10%, except for lifetimes in the ns time range which are less reliable due to the 1 ns time base of the experiment and thus represent lower limits.

Förster Resonance Energy Transfer.

The Förster distance R_0 (the distance at which the energy transfer efficiency is 50%) can be calculated according to the simplified equation^{S17}

$$R_0 = 0.211[\kappa^2 n^{-4} \Phi_D J(\lambda)]^{1/6} \quad (\text{S1})$$

with κ^2 being the orientation factor, n the refractive index of the medium, Φ_D the fluorescence quantum yield of the donor in the absence of acceptor, and $J(\lambda)$ the overlap integral of the donor emission and the acceptor absorption spectra. By employing this equation, R_0 is calculated for array **or** as 70.8 Å, with $\kappa^2 = 2.32$ (using the angles of the dipole moments from the respective structure obtained from molecular modeling shown in Figure 2 and Figure S8), $n(\text{CH}_2\text{Cl}_2) = 1.4240$, $\Phi_D \sim 1.00$ ^{S18} and $J(\lambda) = 2.53 \times 10^{15} \text{ M}^{-1} \text{ cm}^{-1} \text{ nm}^4$. Values of $R_0 = 74.5 \text{ Å}$ for array **rg** (with $\Phi_D = 0.96$)^{S9a} and of $R_0 = 58.7 \text{ Å}$ for array **og** (with $\Phi_D \sim 1.00$)^{S18}, respectively, have been obtained by employing values of $\kappa^2 = 2.41$ and $J(\lambda) = 3.43 \times 10^{15} \text{ M}^{-1} \text{ cm}^{-1} \text{ nm}^4$ for array **rg** and $\kappa^2 = 2.39$ and $J(\lambda) = 8.08 \times 10^{14} \text{ M}^{-1} \text{ cm}^{-1} \text{ nm}^4$ for array **og** (see Table 1).

Furthermore, the rate of energy transfer from a donor to an acceptor can be calculated using the following equation:

$$k_{ET} = \frac{1}{\tau_D} \left(\frac{R_0}{r} \right)^6 \quad (\text{S2})$$

where r denotes the center-to-center distance of the donor and acceptor transition dipole. The latter was afforded from the molecular structures obtained with molecular modeling depicted in Figure 2 and Figure S8, affording values of $r = 19.9 \text{ Å}$ for array **or**, $r = 20.1 \text{ Å}$ for array **rg**, and $r = 20.0 \text{ Å}$ for array **og**. This leads to calculated values for the energy transfer rate of $k_{ET} = 5.9 \times 10^{11} \text{ s}^{-1}$ for **or**, of $k_{ET} = 4.0 \times 10^{11} \text{ s}^{-1}$ for **rg**, and of $k_{ET} = 1.9 \times 10^{11} \text{ s}^{-1}$ for **og**. The afforded values excellently resemble the experimentally obtained rate constants of $k_{ET} = 6.4 \times 10^{11} \text{ s}^{-1}$ for **or**, of $k_{ET} = 4.0 \times 10^{11} \text{ s}^{-1}$ for **rg**, and of $k_{ET} = 1.5 \times 10^{11} \text{ s}^{-1}$ for **og** (see Table 3). Thus, the molecular structure obtained from modeling provided the correct spatial orientation of the chromophores to explain the energy transfer rates by the Förster theory.

References

- (S1) (a) Würthner, F.; Sautter, A.; Schilling, J. *J. Org. Chem.* **2002**, *67*, 3037–3044. (b) Würthner, F.; Thalacker, C.; Sautter, A.; Schärfl, W.; Ibach, W.; Hollricher, O. *Chem. Eur. J.* **2000**, *6*, 3871–3886.
- (S2) (a) Würthner, F.; Stepanenko, V.; Chen, Z.; Saha-Möller, C. R.; Kocher, N.; Stalke, D. *J. Org. Chem.* **2004**, *69*, 7933–7939. (b) Fuller, M. J.; Sinks, L. E.; Rybtchinski, B.; Giaimo, J. M.; Li, X.; Wasielewski, M. R. *J. Phys. Chem. A* **2005**, *109*, 970–975.
- (S3) (a) Kaiser, H.; Lindner, J.; Langhals, H. *Chem. Ber.* **1991**, *124*, 529–535. (b) Nagao, Y.; Naito, T.; Abe, Y.; Misono, T. *Dyes Pigm.* **1996**, *32*, 71–83.
- (S4) Würthner, F.; Sautter, A.; Schmid, D.; Weber, P. J. A. *Chem. Eur. J.* **2001**, *7*, 894–902.
- (S5) Lukas, A. S.; Zhao, Y.; Miller, S. E.; Wasielewski, M. R. *J. Phys. Chem. B* **2002**, *106*, 1299–1306.
- (S6) Prins, L. J.; Jolliffe, K. A.; Hulst, R.; Timmerman, P.; Reinhoudt, D. N. *J. Am. Chem. Soc.* **2000**, *122*, 3617–3627.
- (S7) Hippus, C.; Schlosser, F.; Vysotsky, M. O.; Böhmer, V.; Würthner, F. *J. Am. Chem. Soc.* **2006**, *128*, 3870–3871.
- (S8) Hippus, C.; van Stokkum, I. H. M.; Zangrando, E.; Williams, R. M.; Würthner, F. *J. Phys. Chem. C* **2007**, *111*, 13988–13996.
- (S9) (a) Gvishi, R.; Reisfeld, R.; Burshtein, Z. *Chem. Phys. Lett.* **1993**, *213*, 338–344. (b) Demas, J. N.; Grosby, G. A. *J. Phys. Chem.* **1971**, *75*, 991–1024. (c) Sens, R.; Drexhage, K. H. *J. Luminescence* **1981**, *24*, 709–712.
- (S10) Vergeer, F. W.; Kleverlaan, C. J.; Stufkens, D. J. *Inorg. Chim. Acta* **2002**, *327*, 126–133.
- (S11) (a) van Stokkum, I. H. M.; Larsen, D. S.; van Grondelle, R. *Biochim. Biophys. Acta* **2004**, *1657*, 82–104. (b) van Stokkum, I. H. M.; Lozier, R. H. *J. Phys. Chem. B* **2002**, *106*, 3477–3485. (c) Mullen K. M.; van Stokkum I. H. M. *J. Statistical Software* **2007**, *18*. URL <http://www.jstatsoft.org/v18/i03/> (d) Global and target analysis can be performed with, e.g., the R package TIMP, see <http://cran.r-project.org/doc/packages/TIMP.pdf>.
- (S12) (a) Ford, W. E.; Kamat, P. V. *J. Phys. Chem.* **1987**, *91*, 6373–6380. (b) Ford, W. E.; Hiratsuka, H.; Kamat, P. V. *J. Phys. Chem.* **1989**, *93*, 6692–6696.

(S13) Prodi, A.; Chiorboli, C.; Scandola, F.; Iengo, E.; Alessio, E.; Dobrawa, R.; Würthner, F. *J. Am. Chem. Soc.* **2005**, *127*, 1454–1462.

(S14) (a) Lukas, A. S.; Zhao, Y.; Miller, S. E.; Wasielewski, M. R. *J. Phys. Chem. B* **2002**, *106*, 1299–1306. (b) Shibano, Y.; Umeyama, T.; Matano, Y.; Tkachenko, N. V.; Lemmetyinen, H.; Imahori, H. *Org. Lett.* **2006**, *8*, 4425–4428.

(S15) Pullerits, T.; Heck, S.; Herek, J. L.; Sundström, V. *J. Phys. Chem. B* **1997**, *101*, 10560–10567.

(S16) (a) Asahi, T.; Ohkohchi, M.; Matsusaka, R.; Mataga, N.; Zhang, R. P.; Osuka, A.; Maruyama, K. *J. Am. Chem. Soc.* **1993**, *115*, 5665–5614. (b) Imahori, H.; Hagiwara, K.; Aoki, M.; Akiyama, T.; Taniguchi, S.; Okada, T.; Shirakawa, M.; Sakata, Y. *J. Am. Chem. Soc.* **1996**, *118*, 11771–11782. (c) Tan, Q.; Kuciauskas, D.; Lin, S.; Stone, S.; Moore, A. L.; Moore, T. A.; Gust, D. *J. Phys. Chem. B* **1997**, *101*, 5214–5223. (d) Armaroli, N.; Accorsi, G.; Song, F.; Palkar, A.; Echegoyen, L.; Bonifazi, D.; Diederich, F. *ChemPhysChem* **2005**, *6*, 732–743.

(S17) Förster, T. *Ann. Phys.* **1948**, 55–75.

(S18) You, C.-C.; Dobrawa, R.; Saha-Möller, C. R.; Würthner, F. *Top. Curr. Chem.* **2005**, *258*, 39–82.